2018

Achieving improved leaf area index estimations from digital hemispherical imagery through destructive sampling methods

BOSTON UNIVERSITY

GRADUATE SCHOOL OF ARTS AND SCIENCES

Thesis

ACHIEVING IMPROVED LEAF AREA INDEX ESTIMATIONS FROM DIGITAL HEMISPHERICAL IMAGERY THROUGH DESTRUCTIVE SAMPLING METHODS

by

TIMOTHY DENNIS CONDON

B.S., University of Wisconsin – Eau Claire, 2015

Submitted in partial fulfillment of the

requirements for the degree of

Master of Arts

2018

Approved by

First Reader _____

Alan H. Strahler, Ph.D.
Professor *Emeritus* of Earth & Environment

Second Reader _____

Pamela Templer, Ph.D.
Professor of Biology

Third Reader _____

Crystal B. Schaaf, Ph.D.
Professor of Remote Sensing/GIS
University of Massachusetts – Boston

DEDICATION

My friends and family made me who I am today. Without their continued support none of this work would have been possible.

ACKNOWLEDGMENTS

Firstly, I'd like to express my sincere gratitude to my advisor Dr. Alan Strahler. His continuous teachings, support, and endless patience guided me along the way and made this work possible. My committee members Dr. Pamela Templer and Dr. Crystal Schaaf provided valuable feedback for this work. None of this work would be possible without the support of the Terrestrial Laser Scanning Research Coordination Network (TLSRCN). The TLSRCN not only supported me throughout my graduate degree but was also instrumental in the work for this thesis by organizing the Harvard Forest Calibration Scanning Activity. Dr. Dave MacFarlane at Michigan State University, Dr. Phillip Radtke at Virginia Tech, and Jereme Frank at the University of Maine and their forestry crews provided all destructive sampling data and field work and were always ready to respond to my queries. Dr. Kim Calders and Mat Disney at Ghent University and University College London provided TLS data results that made this project possible. Dr. Will Woodgate provided timely advice and knowledge to help clarify the complex issue of wood area index in this study. Finally, I'd like to express my profound gratitude to my parents who always make me feel special and have made me the man I am today, Emily who was always patient with my frustrations as I worked from home staying up late, my roommates throughout my graduate degree who kept me sane and provided me a valuable outlet aside from school, and Doris, who was always there to keep me calm and help me relax when needed.

ACHIEVING IMPROVED LEAF AREA INDEX ESTIMATIONS FROM DIGITAL HEMISPHERICAL IMAGERY THROUGH DESTRUCTIVE SAMPLING METHODS

TIMOTHY CONDON

ABSTRACT

Destructive sampling of 20 trees of four tree species in a mixed New England conifer/hardwood stand shows that leaf area comprises 72, 77, and 78 percent of plant area as measured with digital hemispherical photography of the stand in (1) leaf-off, (2) leaf-out and pre-harvest, and (3) leaf-out and post-harvest conditions. Leaf area index values for the stand, estimated through destructive sampling, were 4.42, 5.98, and 5.08 respectively, documenting the progression of leaf growth through post-harvest. Terrestrial lidar scans (TLS) of the stand in (1) leaf-off and (2) leaf-out and pre-harvest conditions provided leaf area index values of 4.49 and 6.00 using the correction applied to observed plant area index, showing good agreement. The method relies on destructive sampling to relate the weight of foliage removed from sample trees to leaf area and fine twig area within the foliage as measured by a flatbed scanner. Two conifer species, eastern hemlock and white pine, and two deciduous species, red maple and red oak, in five diameter-size classes, were harvested from the 50 x 50-m stand in late summer. Leaf and twig areas of these trees provided species-specific allometric equations relating stem basal area to leaf and twig area, and a stand map provided species, counts and diameters of all trees in the plot. These data then allowed estimation of the leaf area of the stand as a whole for comparison with optical methods. The ratios of leaf to fine-branch area for

each species vary, with values of 5.33, 25.38, 260.88 and 140.35 for eastern hemlock, white pine, red maple, and red oak respectively. This variance shows that woody-to-total area constants, which are used for calculating leaf area index from plant area index values determined by optical gap probability methods, will be quite dependent on stand composition and questions the common usage of literature constants for this purpose. This study shows how destructive sampling can lead to better estimation of forest leaf area index and wood area index from hemispherical photography and terrestrial lidar scanning, which has the potential to improve modeling of nutrient cycling and carbon balance in ecosystem models.

TABLE OF CONTENTS

LIST OF TABLES

LIST OF FIGURES

LIST OF ABBREVIATIONS

BU ..... Boston University

DHP..... Digital Hemispherical Photography

FIA ..... Forest Inventory and Analysis

GPP ..... Gross Primary Production

LAI..... Leaf Area Index

MSU ..... Michigan State University

NPP ..... Net Primary Production

PAI ..... Plant Area Index

PAVD..... Plant Area Volume Density

RCN ..... Research Coordination Network

RGB ..... Red Green Blue

SLA ..... Specific Leaf Area

STA ..... Specific Twig Area

TAI..... Twig Area Index

TLS ..... Terrestrial Lidar Scanning

TRAC..... Tracing Radiation and Architecture of Canopies

VAI ..... Vegetation Area Index

WAI..... Wood Area Index

INTRODUCTION

Forests and Carbon Flux

The contribution of temperate forests to the global carbon budget is dynamic, both spatially and temporally. Throughout a given year, forests are either an atmospheric carbon source or sink due to phenology and climate. Temperate deciduous forests during the winter and leaf-off period are a source of carbon due to respiration of the woody biomass, including roots and stems. In the spring, a transition occurs where the deciduous leaves begin to develop and photosynthesize and evergreen leaves become active as well. This transition turns an entire forest ecosystem from a carbon source to a sink within several weeks. These forests provide a large terrestrial CO_2 flux in the carbon cycle. Because of this magnitude, it is very important to further understand how leaves and forest structure affect the ability of a forest to take up carbon.

Gross Primary Production (GPP) is a measure of total photosynthesis and will vary seasonally as the leaves cycle through development, maturity, and senescence. Net Primary Production (NPP) measures the net amount of carbon flux occurring. It is defined as the difference between GPP and Respiration (R) of the total ecosystem. As NPP is the total amount of flux occurring in a system, looking at the sign convention and amount of NPP flux illustrates changes in CO_2 concentrations in the atmosphere. It will be negative when the forest ecosystem is a source of CO_2 and positive when it is a sink. LAI is used as a measurement of biomass of leafy (photosynthetically active) material in the forest canopy and is a key structural parameter that controls energy, carbon, and water fluxes in forests; it is defined typically as one-sided leaf area per unit of ground area

(Jonckheere et al., 2004). LAI is variable throughout the year from green-up to senescence, and its variation provides a key input to modeling carbon fluxes in forests.

Plant canopy function is a fusion of complex structural and biophysical processes. These processes range from nutrient cycling to leaf orientation to herbivory. The total amount of photosynthetically active material is an ecological characteristic that is influenced by, and in turn, influences many of these factors. Canopy leaf area is seen as a dominant control over transpiration, energy exchange, and GPP (Asner et al., 2003). Leaf area is thus used in many global and local ecological models (Bondeau et al., 2008). As a dimensionless quantity, LAI is used in models and studies at a wide range of spatial scales and has become a key descriptor of forest structure (Asner et al., 1998).

Reich (2012) examined the links of carbon fluxes and forest canopy attributes, similarly to what is proposed here. Forest stand productivity was examined as a function of the capacity of the stand to harvest light and to fix carbon biochemically. LAI was used as a proxy of the capacity to harvest light, while nitrogen concentration was examined as the biochemical carbon fixing capacity. LAI and percent nitrogen were able to explain 75 percent of the variation in net primary productivity (NPP) of above-ground biomass in forests. Gower et al. (1999) state that the proper way of scaling LAI, absorbed photosynthetically active radiation, and NPP varies greatly depending on the ecosystem, further reinforcing the idea that this is a complex problem that requires added studies to better understand specific ecosystems. They also state that estimates observed by satellite are correlated with ground estimates of LAI and NPP, though there is much to be further understood in how to globally model these parameters using satellite optical imagery.

Studies performed by Forkel et al. (2016) and Graven et al. (2013) found that exchange of CO_2 is amplified in northern ecosystems. They state this is due to greater land area in northern latitudes when compared to the southern hemisphere, leading to higher overall plant productivity variation as GPP increases in vegetated areas. This leads to more seasonal CO_2 variability between leaf-on and leaf-off seasons. As plants are drivers of CO_2 uptake in terrestrial ecosystems and a major part of the climate-vegetation-carbon cycle feedback, it is more important now than ever to focus on developing a deeper understanding of plant structure and photosynthetic material. Khomik et al. (2013) observed a linear relationship between LAI and GPP at their temperate mixed forest research plot, thus pointing to the importance of LAI and forest structure in climate science. Multi-factor experiments are key to developing robust studies of carbon storage and exchange (Templer and Reinmann, 2011).

Leaf Area Index

Leaf area index (LAI) was first defined as a dimensionless variable representing the total one-sided area of photosynthetic tissue per unit ground area by Watson (1947). While this definition is clear when thinking of broadleaf species, which have two sides with similar surface areas, it is less useful when considering needleleaf species with triangular, cylindrical, or semicylindrical leaves. To account for this, in the current literature LAI is defined as one-half the total leaf area per ground surface area (Chen and Black, 1992, Myneni et al, 1997, Jonckheere et al., 2004) or, for computational purposes, the maximum projected leaf area per ground surface area (Myneni et al., 1997).

LAI is one of the most important primary descriptor variables used for carbon balance modeling and surface radiation models both regionally and globally (Hyde et al., 2006). This arises because radiative transfer between the plant and the atmosphere, which governs evapotranspiration and photosynthesis rates, takes place on and through leaf surfaces (Running, 1984, Law et al., 2001). Thus, LAI is an essential climate variable, and is used in many models to track climate-driven changes in global biogeochemical cycles (Myneni et al., 1997, Nemani et al., 2003, Garrigues et al., 2008, Woodgate et al., 2015). Change in phenology of forest and other land covers is one of the main indicators of climate change and can be tracked by examining LAI over time (Bequet et al., 2011, Calders et al., 2015).

LAI is a variable that varies greatly over time, space, and species composition. Even for a single specimen, specific leaf area (SLA), defined as the ratio of green leaf area to dry leaf weight, varies throughout the height of the canopy, making it difficult to determine total LAI (Niinemets and Kull, 1995). Combining this inherent variance with variations in measurement methods can lead to wide variations in final determined LAI values. Using a light interception method that will be further discussed below, Welles and Norman (1991) found that simple changes in sky brightness can cause LAI measurement variations by up to 10 percent. The various methods to assess LAI can be grouped into two main categories: direct sampling and indirect measures.

Direct Sampling

Direct methods are the most accurate way to determine LAI. They principally involve collection of leaves of either subsamples or full canopies. Direct sampling can

involve litterfall collection, destructive sampling, or point-contact sampling. A separate, gravimetric approach may also be used to determine LAI. This approach is based on determining the specific leaf area (SLA, or ratio of green leaf area to dry weight, as noted earlier). The SLA is typically determined from subsamples of leaves collected from destructive sampling or litterfall. Coupled with wet leaf weights and ratios of wet-to-dry weight from laboratory analysis, SLA values by species then provide leaf areas of individual trees from destructive sampling or of canopy leaf areas from litterfall. For destructive sampling of individual trees, the sampling plan will typically provide a method for extrapolating leaf areas from harvested individuals to the stand as a whole. The gravimetric approach is typically used with larger leaf samples where it is easier to perform. However, the leaf sample should be mixed from all parts of the canopy in order to better account for SLA variations between branch age, canopy height, and light exposure (Niinemets, 1997). While being the most accurate, these direct sampling methods may be destructive to the vegetation being studied and are typically more time consuming and costly (Weiss et al., 2004).

Indirect Measures

Ground-based indirect measures of obtaining LAI involve various remote sensing methods. These indirect measures include digital hemispherical photography (DHP), TRAC instruments (Tracing Radiation and Architecture of Canopies) (Jonckheere et al., 2004), and terrestrial lidar scanning (TLS). All of these methods typically rely on identifying gaps in the canopy and use gap probability (P_{gap}) to retrieve an effective LAI, although there are some exceptions. The P_{gap} method is based on sampling the probability

of gap to the sky as a function of the view zenith angle from a fixed ground point (Jupp et al., 2009). Determining LAI through P_{gap} utilizes a negative exponential attenuation model of a ray along a path through a canopy, while taking into account a model of leaf angle distribution with changing zenith angle (Zhao et al., 2011).

$$P_{\text{gap}}(\theta, z) = \mathrm{e}^{-G(\theta)L(z)/\cos\theta}$$

LAI found this way is labeled as an "effective LAI" due to an implicit assumption of random distribution of leaf centers. Because leaves are clustered on branchlets (i.e., are clumped), effective LAI normally underestimates true LAI. A measurable canopy clumping function (λ) can be used to correct for clumping (see Section 2.3.1). The clumping parameter accounts for nonrandom placement of leaves, in which leaves are absent between tree crowns, absent within holes inside crowns, and clumped within leaf clusters on branches. Jupp et al. (2009) presented a model for dealing with clumping using full-waveform TLS. Zhao et al. (2012) utilized this method using the Echidna Validation Instrument (EVI) TLS system to determine the clumping index and compare effective LAI and true LAI.

Even with the clumping factor included, LAI achieved through P_{gap} isn't the true LAI value of the canopy. Gap fraction methods cannot separate woody and leafy materials in the canopy. Therefore, it is more appropriate to label the results of the gap fraction analysis as a plant area index (PAI) (Neumann et al., 1989, Chen et al., 1997). Woodgate et al. (2016) developed a method using classified DHP to separate woody and leafy materials in the PAI using a system based upon the methods of Sea et al. (2011). Calders et al. (2018) compared and developed methods to remove the effects of large

woody material on LAI using DHP, TLS, and a commercially used LAI sensor, the LiCOR LAI-2000 and its newer version, LAI-2200. They found that average effective PAI estimates were 27 percent higher than effective LAI estimates. However, they observed a large difference in the results from these instruments, showing that future work needs to be done on removing woody material effects on LAI.

Because the plant area index includes both leafy and woody materials, we can separate them as

$$PAI = WAI + LAI$$

where WAI is the wood area index and defined as one-half of the surface area of trunks and branches. Several methods have been implemented to separate WAI and LAI. Dual-wavelength, full-waveform TLS utilize two different wavelengths and reflectance levels of wood and leaves to aid in the separation of beam returns into wood and leaf hits. Li et al. (2013, 2015, 2016), Howe et al. (2015), and Douglas et al. (2015) all demonstrated this method using the dual wavelength Echidna lidar (DWEL). Beland et al. (2014) proposed using voxelization of TLS returns to separate leaves from woody material in the canopy.

Woodgate et al. (2015) compared several indirect measures of determining LAI using high resolution DHP, low resolution DHP, and a Riegl VZ-400 commercial TLS instrument. They found the level of variability among these results to be greater than desired uncertainty levels. Despite this uncertainty, indirect optical measures of LAI from hemispherical imaging and laser scanning are likely to be the way of the future for global

LAI validation, as they are significantly faster and cheaper than direct destructive sampling.

MATERIALS AND METHODS

Study Overview

Introduction

This research exploits an unusual opportunity to validate retrievals of leaf and plant area index (LAI, PAI) of a forest stand from digital hemispherical photography (DHP) by destructive sampling of forest trees. In 2016, the Terrestrial Laser Scanning Research Coordination Network (RCN) began planning a calibration activity at the Harvard Forest, in Petersham, Massachusetts, to take place with the help of the Forest in 2017 (Strahler et al., 2017, SilviLaser2017 Proceedings). The activity, which coupled TLS scanning with destructive sampling of a selection of scanned and harvested trees, was designed to examine the following questions:

- How accurate are estimates of the woody volume and above-ground biomass of forest trees that are obtained from terrestrial laser scanning (TLS) and associated retrieval algorithms?
- Can TLS improve the precision of stand-based biomass estimation and provide accurate allometric equations from virtual volume and biomass estimates?
- How well do TLS instruments estimate leaf area, leaf biomass, and the foliage profile of leaf area with height?

The field calibration experiment focused on a forest stand of mixed conifers and hardwoods in the Tom Swamp Tract of the Harvard Forest, Petersham, Massachusetts. A main plot of 50 by 50 m, along with two smaller accessory clusters of trees, was selected

and scanned in August, 2017, by both commercial (Riegl VZ-400, Faro Focus, Geoslam Zebedee Zeb1) and research instruments (Salford Advanced Laser Canopy Analyser, SALCA; Compact Biomass Lidar, CBL; Portable Canopy Lidar, PCL) at varying scan settings and scan location plans. Following scanning, 20 trees were harvested for destructive sampling to measure volume and biomass from dimensional measurements and weights of trunks, stems, branches, and leaves, as well as wet and dry wood-density measurements of tree components. The main plot was also scanned with a Riegl VZ-400 in April, 2017, while deciduous trees were leafless, as a comparison benchmark. At the present time (March 2018), data processing of TLS scans and destructive samples is close to completion. The TLS RCN includes about 75 participants and is supported by a grant from the National Science Foundation (NSF) to Boston University (DBI-1455636)[1]; leafless scanning was provided by UNAVCO, also with NSF support[2]. (NSF/NASA EAR-0735156).

Main Plot

The stand selected for the calibration activity was located in the Tom Swamp tract of the Harvard Forest. This stand lies within an area allocated to harvest for Harvard Forest use as firewood and lumber. This research uses data from the main plot, a 50-m by

---

[1] RCN-IDBR: Coordinating the Development of Terrestrial Lidar Scanning for Forest Carbon Inventory and Ecological Applications, DBI-1455636.

[2] UNAVCO is a non-profit university-governed consortium that facilitates geoscience research and education using geodesy. Supported by NSF/NASA EAR-0735156.

50-m inner plot with an adjoining 10-m buffer on all four sides, which was staked and labeled on a 5-m grid (Appendix Figure 16). Four tree species, eastern hemlock (*Tsuga canadensis*), eastern white pine (*Pinus strobus*), northern red oak (*Quercus rubra*), and red maple (*Acer rubrum*), account for more than 90 percent of the basal area. Also present are birch (*Betula spp*.) and a large white oak (*Quercus alba*). Eastern hemlock is the dominant species with 55 percent of the total basal area. The dominance of eastern hemlock has suppressed development of the understory in the stand, making the stand relatively open at ground level and more accessible to scanning and harvesting activities.

Before harvest, a map with accompanying inventory of all stems in the plot greater than 1 inch (2.5 cm) in diameter was prepared. Using the staked grid, each tree stem was located in grid coordinates using distance and compass azimuth from the nearest stake to the southwest (Appendix Figure 16). Attributes of species name, DBH, and canopy class according to FIA protocol (open growth, dominant, codominant, intermediate, and suppressed) were recorded for each stem. Each stem was numbered and tagged for future reference. Table 1 provides brief summary statistics for the stand; Appendix Table 10 provides stem information for the total plot.

Table 1. Tree Basal Areas.

Species	Mean DBH (cm)	Percentage of total plot Basal Area
Eastern Hemlock	22.29	55.49%
Birch	8.30	1.13%
Red Maple	19.59	7.84%
Red Oak	26.80	17.36%
White Pine	35.90	7.30%
White Oak	39.80	0.88%
Dead Trees	14.76	10.00%

Objectives of the Study

Ground-based hemispherical photography of forests has been used for many years to quantify forest structure (Jonckheere et al., 2004). Given the wide range of data available from the RCN calibration activity, it is possible to increase the understanding of the accuracy and utility of forest structure measurements retrieved from DHP, which is a much simpler and less costly technology than TLS. One canopy property commonly retrieved from DHP is leaf area index (LAI). However, this process requires a number of theoretical adjustments as described in following sections. Validation of LAI from DHP requires actual measurement of leaf area, which is costly and time consuming and rarely done.

However, with the more detailed destructive sampling acquired during the Harvard Forest RCN calibration activity, it is possible compare retrieved LAI to LAI derived from direct leaf area measurements in order to assess accuracy and bias. In addition, the destructive sampling data provide, for the first time, a set of quantitative measurements of fine branch area within leaf clusters. These measurements yield a set of species-specific ratios of the area, volume, and weight of destructively sampled leaves to small twigs attached to these leaves. The ratios allow a better understanding of within-crown clumping between the fine branches and the leaves and allows for separation of fine-branch woody area from leaf area to give true LAI values.

TLS processing also provides a pathway to estimate PAI. Using a similar optical approach to DHP, but in three dimensions instead of two, each TLS scan can retrieve

both the total-canopy PAI and a foliage profile of foliage area volume density with height. Comparison of DHP- and TLS-derived PAI with respect to destructively-sampled estimates of PAI and LAI also adds information to the value added by having the third dimension.

Terrestrial Lidar Scanning

Multiple TLS scans were acquired from the 50 by 50-m main plot. On April 24, 2017, the plot was scanned on a 10-m grid, with 12 additional scans outside the plot also acquired to reduce occlusion effects on the plot edge. These positions can be seen in Figure 1. The scans were acquired by UNAVCO using a Riegl VZ-400. This set of scans provided deciduous leaf-off data with minimal occlusion. Although several TLS instruments were deployed in the plot in mid-August as part of the calibration activity, here only data from the Riegl VZ-400 is considered and was provided and operated by researchers from University College London, which scanned the plot August 17-18. The August scan performed by UCL was designed to match the scan performed by UNAVCO (Figure 1) to ensure comparability of the two datasets and results.

The Riegl VZ-400 operates at a 1550 nm wavelength within the shortwave infrared, has a range of over 300-m, and has a beam divergence of 0.35 mrad. Methods similar to Calders et al. (2018) were used to approximate the gap probability with height. PAI was then found using the linear model of Jupp et al. (2009) to estimate PAI at the zenith ring between 55° and 60°. This processing was carried out by Kim Calders at Ghent University using pylidar, an open-source python tool (www.pylidar.org).

Destructive Sampling

The destructive sampling portion of the project was conducted with the support of the U.S. Department of Agriculture's Forest Inventory and Analysis (FIA) program. The goal of this program is to measure and monitor changes in U.S. forest biomass and carbon stocks through time. This portion of the project was led by Dr. David MacFarlane at Michigan State University (MSU), Dr. Philip Radtke at Virginia Tech (VT), and Jereme Frank at the University of Maine (UMaine). Eastern hemlock, northern red oak, red maple, and eastern white pine are four species that are a part of the larger FIA national biomass equation project, making the plot at Harvard Forest of strong interest to the FIA analysis.

A total of 16 trees were felled for sampling from the 50 by 50-m plot, with four individuals from each species in varying size classes as seen in Table 16 (p. 71-72). The trees were selected to fill out the FIA project needs. Each species harvested included one tree in each of four of the five chosen size classes (1, 2, 3, and 5). Four additional trees, one per species, from size class 4 were also harvested at a location about 30 m from the plot, giving a grand total of 20 sampled trees.

Trees were sampled according to a protocol developed by MSU's Department of Forestry. Of particular interest to this study is how detailed live branch measurements are acquired. Every branch greater than one inch (2.5 cm) in diameter attached to the stem is declared a primary branch and numbered and cut from the stem. Measurements of diameter just above the junction with the stem, the height of the branch separation from the tree base, and whether or not the branch was dead or alive were taken as well.

Secondary branches, defined as branches originating from primary branches, were also marked, cut, and removed from primary branches. Trunks and branches were then cut into segments of about 4-ft. Each segment was weighed and the diameters of each segment at each end and at the midpoint were acquired. A short section of the middle of each primary branch segment (referred to as a "mid") was also removed for measurement of wood density. Mid samples for wood density of the largest secondary branch on any primary were taken as well.

All live secondary branches were then split off to obtain leaf measurements. The leaves of these branches were clipped with some small twigs still attached to the leaf. The combination of these leaves and small twigs were weighed and recorded. A ten percent subsample of this leaf and twig mixture was then taken to the lab to be dried, separated, and weighed. The hardwood samples, in this case, red oak and red maple, had their leaves and fine twigs separated prior to oven-drying. The leaves were dried between 65° and 70°C, while the twigs were dried at 105°C. Softwood samples, the hemlock and white pine, had their needles and fine twigs separated after oven drying at 105°C. The needles were then weighed separately after being cooled to an oven dry temperature between 65° and 70°C. The fine twigs from these samples were saved to measure specific twig area (STA).

Specific leaf area (SLA), is defined according to the following equation.

$$SLA = \frac{Green\ Leaf\ Area}{Dry\ Leaf\ Mass}$$

SLA for each harvested tree was found by taking nine samples from each tree. The tree crowns were split into three equal subsections (upper, middle, and lower), and three

leaf/needle samples were taken from each third of the crown. The branches from which these samples were taken were flagged in order to place the leaf measurements accurately within the total tree record. The leaves were then weighed and scanned with a flatbed scanner before they began to lose moisture. The scans were processed in the open software package ImageJ to find the total leaf area. Dry weights, obtained as above, were used to find the SLA of each sample. This gave a specific leaf area in units of square centimeters per gram (cm^2g^{-1}).

Leaves and Twigs

A similar process was used to find specific twig area (STA) as SLA.

$$STA = \frac{Green\ Twig\ Area}{Dry\ Twig\ Mass}$$

Dry weights of the twigs were taken, and the twigs were scanned with a flatbed scanner and analyzed using ImageJ. However, the twigs were scanned after they were dried to a moisture content of approximately 12 percent, which induced wood shrinkage from moisture loss. Thus, it was not possible to measure the green area of the twigs (A_g) directly.

To account for area loss due to moisture in the dry twigs, the following equation (White and Ross, 2014). was used to find the total shrinkage percentage.

$$\Delta d = \sqrt{1 - \Delta v}$$

Here, Δd is the proportional change in diameter and Δv is the volumetric shrinkage proportion at oven-dry conditions. Known oven-dry shrinkage values were used (Table 2).

Table 2. Wood Shrinkage

Species	Volumetric change, percent
Eastern hemlock	9.7
Red maple	12.6
Red oak	13.7
White pine	8.2

This method was used to convert all dry twig areas (Appendix Table 12) into green twig areas in order to calculate STA and allow proper a proper leaf-to-twig area ratio to be found. Using this ratio, it was possible to better account for within-crown clumping.

Digital Hemispherical Photography

DHP and TLS Scan Points

The timber stand selected for destructive sampling is diagrammed in Figure 1 and Appendix Figure 16. The 50-m by 50-m main plot and a 10-m surrounding buffer zone were staked on a 5-m grid, and scan and photo location points were placed on 10-m main plot grid intersections. For TLS, the buffer zone included 8 additional points on its four outer sides, and 4 additional scan points placed at 25 m diagonally outward from the main plot corners. Photo points thus totaled 36, while TLS scan points totaled 48.

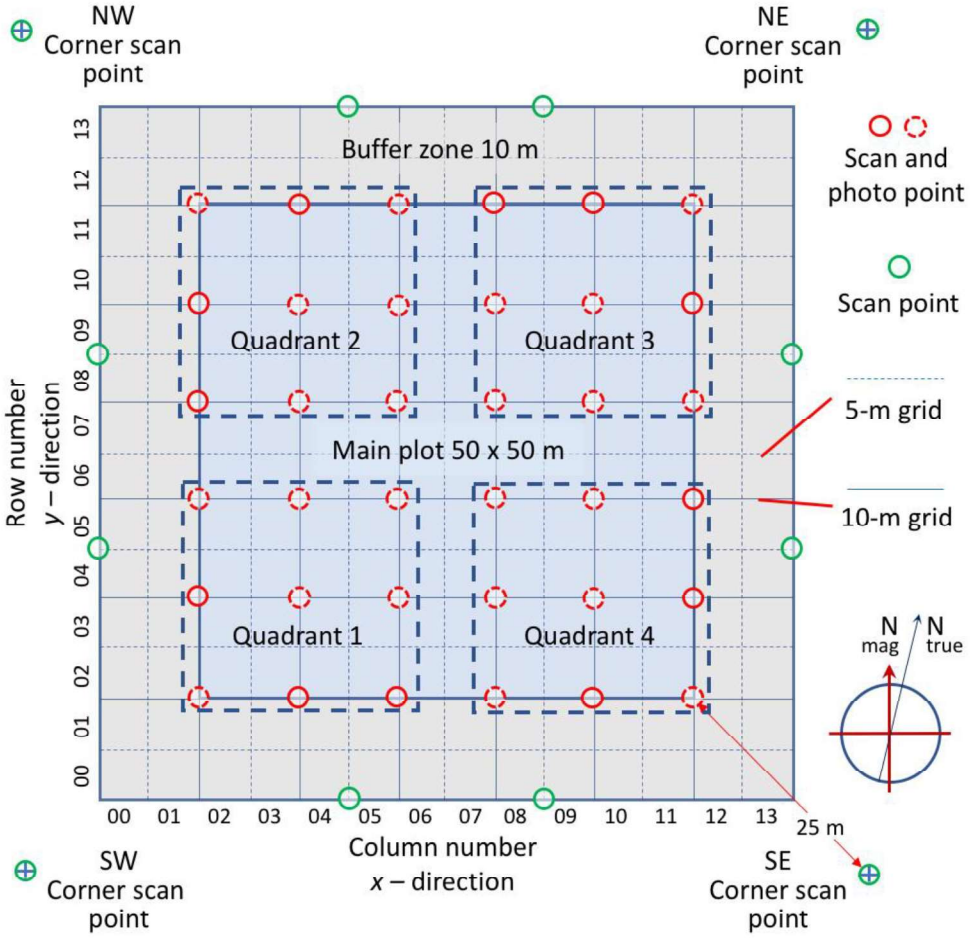

Figure 1. Plot Acquisition Map. Diagram of main plot, showing locations of scan and photo points. The main plot includes 36 scan and photo points; 8 additional scan points are placed in the 10-m buffer zone around the main plot, as well as 4 scan points located 25 m diagonally from the main plot corners. Hemispherical photos were processed by quadrants in groups of 9, as shown. For whole-plot processing, the subset of 24 photo points shown by dashed circles was used.

Data Acquisition Procedures

Digital images were acquired using a Nikon Coolpix 990 camera fitted with the hemispherical (fisheye) lens attachment. The camera was positioned on a leveled monopod or tripod at a height of 1.6 m (matching the height of the TLS instrument). To avoid camera motion, photos were triggered using the time release option.

To provide a more uniform sky field, images were acquired under cloudy conditions. Exposure was determined using a Gossen Digisix light meter in incident mode with diffusing hemisphere in place, pointed upward at the approximate height of the camera at the photo point, just prior to taking the photo. The basic exposure was set to underexpose the image by two *f*-stops (i.e., exposure reduced to 1/4) with respect to the sky, providing a greater contrast between sky and canopy. During times of changing sky conditions (e.g., varying cloud brightness), multiple photos were typically acquired, bracketing the basic exposure by ± 1 *f*-stop. From the bracketed set of three images, the image with the best range of canopy gray tones was selected for processing. Thus, each date was represented by 36 hemispherical digital images on the 10-m plot grid.

DHP Acquisition Dates

Table 3 presents a summary of acquisition dates. The first data acquisition occurred on April 27, 2017, while the deciduous species, primarily red maple and red oak, were still leafless. Images were then acquired throughout the summer season on the dates of June 26, July 25, and on August 9, just prior to the destructive sampling. After the sampling, images were acquired on September 14, well before local senescence. A total of 392 images were acquired, with each set winnowed down to the best exposures at each photo point.

Table 3. Image Acquisition

Acquisition Date	Images Acquired	Canopy Condition
27-Apr-17	75	Leaf-off
26-Jun-17	98	Full foliage
25-Jul-17	73	Full foliage
9-Aug-17	89	Before destructive sampling
14-Sep-17	57	After destructive sampling

Digital Image Processing with CAN-EYE

DHP were processed for PAI using the CAN-EYE software package (v.6.4.6 2017), developed by the French National Institute of Agronomical Research (INRA). CAN-EYE provides for calibration to a custom color camera and fish-eye lens system, in this case the Nikon Coolpix 990 camera with hemispherical lens. Calibration of the software involves identifying the optical center of the lens image and the distance along the radius of the circular image. Using this calibration, CAN-EYE can determine the zenith and azimuth angles of each pixel, thus allowing for proper gap fraction and clumping computation. CAN-EYE also processes up to 25 red-green-blue (RGB) color images together as samples of a single stand in order to provide robust averages of output values.

To provide a measure of spatial variance within the plot, the images were processed in four quadrants of nine photographs (see Figure 1). These quadrants correspond with the quadrants used during the selection of trees for harvest by destructive sampling in order to provide a balanced spatial sampling of the plot. Images were also processed for the plot as a whole for each date, although due to limitations of CAN-EYE

only 24 images were selected from each date. Their locations are identified in Figure 1 by dashed circles and include the sixteen points in the center, the four corner points, and four points on the edges. Processing this way gives a five sets of CAN-EYE values for each date: one set for each quadrant and one total plot set.

CAN-EYE works by estimating the gap probability associated with each pixel using the RGB camera color information. Utilizing a multispectral classification algorithm with operator guidance, two classes of pixels are identified: background (sky, P0 = 1) and vegetation (P0 = 0). The remaining pixels are considered mixtures of background and vegetation and classified as mixed pixels. The color of each mixed pixel is linearly interpolated between the colors of background and vegetation to estimate the fractional gap probability. The pixel-based gap probability measurements are averaged over all azimuth values within 2° zenith rings, yielding average gap probability with zenith angle.

The distribution of gap probabilities by zenith angle is then fitted to an elliptical leaf angle distribution model that assumes a random placement of leaf/plant facets in the canopy as well as perfectly diffuse scattering by individual facets. The method inverts the model using a precalculated lookup table based on forward calculations of gap probability with zenith angle, given increments of leaf area index and average leaf angle (Section 2.3.1).

Prior to the classification step, masks were placed in the imagery to cover areas not corresponding to vegetation or sky. These masks covered objects such as range poles marking positions in the study plot, an occulting disk sometimes used to block the sun

from causing lens flare, and human interference. These masked areas are removed by CAN-EYE in processing. When classifying image pixels, sky and vegetation classes were kept as inclusive as possible, limiting mixed pixel classifications to a maximum of 10 percent of mixed pixel presence.

CAN-EYE outputs retained for this study are shown below. Here we note that while theory may refer to LAI, the values retrieved are best regarded as PAI values, since branches also intercept skylight and reduce the gap probability.

- PAI57: The plant area index derived from the 56–58° zenith ring. At a 57° zenith angle, theory shows that LAI is nearly independent of leaf angle distribution. This provides a good first estimate of PAI.
- PAIeff: Effective plant area index. This is the PAI retrieved from the best fit of the observed gap probabilities with zenith angle to the entries in the modeled lookup table. It is an "effective" value, since it is derived with the assumption of random spatial placement of plant facets and thus does not accommodate clumping of plant facets.
- ALAeff: Average leaf inclination angle. It is also retrieved from the best-fit entry in the modeled lookup table, and is an effective value based on assumptions of random placements of leaf facets.
- CF: Clumping factor (clumping index). This factor estimates the ratio of effective plant area index to the true plant area index. Since clumping acts to hide plant facet area, the true PAI will be greater than the effective PAI and the clumping index will be less than unity. The estimate captures

clumping created by large voids between tree canopies and some smaller voids within tree canopies, but does not detect fine-scale leaf clumping at the branchlet or shoot level.

- PAItrue: True plant area index. This is the PAI corrected for clumping. To find it, a new set of gap probability lookup values indexed by PAI and ALA is modeled with the clumping factor included. The true PAI is then taken as the value retrieved from the best-fit entry of the observed gap probabilities to the model predictions using the clumping factor.
- ALAtrue: True average leaf angle. As in PAItrue, this value is corrected for clumping using the same method.

Estimating LAI from Hemispherical PAI

Gap Probability Theory for Leaf Area Index

Estimating leaf area index with hemispherical photography uses a variant of negative exponential attenuation theory, which is based on attenuation of a light beam passing through a scattering and absorbing medium of randomly-placed very fine particles (e.g., molecules in a gas) that interact with the beam. Applying this theory to a canopy of leaf facets, we can write (following Weiss et al., 2004):

$$P_0(\theta_v) = e^{-\frac{\lambda G(\mu_v) L}{\mu_v}}$$

$$L = -\frac{\mu_v}{\lambda G(\mu_v)} ln[P_0(\theta_v)]$$

where θ_v is the view zenith angle; μ_v is the cosine of θ_v; $P_0(\theta_v)$ is the gap probability, or the probability that a ray beam will exit the canopy at view zenith angle θ_v; $G(\mu_v)$ is the projected area in direction θ_v of a unit of leaf area contained in a unit of canopy volume; λ is a clumping parameter ($\lambda < 1$); and L is the leaf area index. The clumping parameter accounts for nonrandom placement of leaves, in which leaves are absent between tree crowns, absent within holes inside crowns, and clumped within leaf clusters on branches. These effects increase the observed gap probability, thus underestimating the leaf area that would be derived without the clumping parameter (effective leaf area or PAIeff in CAN-EYE).

From this relationship, it can be seen that an estimate of L requires knowing the projected area function as well as the clumping parameter. $G(\theta_v)$ is fitted to the distribution of gap probability values observed by zenith angle; λ is derived from the spatial pattern of connected gap pixels (i.e., hole sizes) within constant zenith rings superimposed on the hemispherical image. In addition, woody materials in the canopy also reduce the gap probability. Thus, retrieved leaf area should be referred to as plant area (e.g., PAI), unless the retrieved value is further corrected to remove the woody contribution.

Twig-Area Adjustment

As noted above, there are methods that are capable of adjusting for between-crown clumping and larger within-crown gaps in the canopy to find PAItrue. However, the PAI can be further corrected to LAI by removing the woody contribution of fine branches within the crown canopy. This study provides the opportunity to carry this out

by creating a leaf-to-twig area ratio for each species. This quantity was found for each species as the ratio of all leaf area to all twig area for all samples gathered. If *R* is the leaf-to-twig-area ratio, it is then easy to show that since

$$PAItrue = LAI + TAI, \quad R = \frac{LAI}{TAI}$$

we find that

$$TAI = \frac{PAItrue}{R+1}, \quad LAI = PAI - TAI$$

for each species. However, the PAItrue for one or more hemispherical photos will be derived from different species with different leaf-to-twig area ratios, and must be corrected with an average *R* value that is weighted by observing a plot-based *R* value from destructive sampling of both leaves and twigs.

Plot and Species-Specific Allometry from Destructive Sampling

To estimate leaf and twig areas of individual trees in the plot, as well as the leaf area of the canopy as a whole, simple allometric equations were derived for all four species, relating DBH to leaf and twig area. To carry this out, leaf area and twig areas were determined for each destructively-sampled tree using dry leaf and twig weights of the 10-percent sample acquired for each tree. By applying specific leaf and twig areas (SLA, STA) to the weights, leaf and twig areas for each sampled tree were then obtained. These data were used to fit simple exponential models by species for leaf and twig area given DBH:

$$L, T = e^{a} \cdot B^{b}$$

$$\ln L = a + b \ln B$$

where *L, T* is leaf or twig area (m^2), *B* is basal area (cm^2), and *a* and *b* are best-fit constants to the log-linear form of each model. Since leaf and twig areas were obtained by destructive sampling of one tree of each species in each of five size classes, each equation is based on five points.

The LAI and PAI of the plot are then estimated by applying the appropriate allometric equation to predict leaf and twig area for each tree in the plot, summing leaf and twig areas by species, then finding leaf area, twig area, and plant area totals (m^2) for the plot and dividing by the plot area (m^2). Dead trees are omitted in this analysis. A value of the leaf-to-twig area ratio for the entire plot, R_{plot}, is also calculated. With these values in hand, the PAItrue from DHP can be compared to PAI from destructive sampling. Also, PAItrue can be adjusted to LAItrue using R_{plot} and compared to the plot LAI from destructive sampling. The difference may be ascribed to fine-scale branchlet clumping effects remaining in the DHP estimate, anisotropic leaf and branch reflectance, and variance in the proportion of leaf and branch colors in each DHP pixel. This analysis was also performed for DHP for after-harvest conditions based on a modified list of trees remaining in the plot after destructive sampling. That analysis provides an estimate of the leaf area loss in trees felled for the destructive sampling.

RESULTS

Remote Sensing PAI

DHP

DHP pixel classification fractions for the entire plot can be seen in Table 4 and show that leaf-off data was classified as having the most sky pixels and least green pixels

while being the least saturated (saturation value of 8.0 PAI). Conversely, the August 9 acquisition, just before destructive sampling, showed the highest saturation percentage and the least sky percentage classification. These results provided larger DHP PAI values in August than in any other month, which can be seen in Table 5 and Figure 2.

Table 4. DHP Classification

Acquisition Date	Sky %	Green %	Mixed %	Saturated %
27-Apr-17	11.04	80.97	7.99	21.93
26-Jun-17	5.50	87.36	7.14	24.86
25-Jul-17	6.06	87.42	6.52	23.22
9-Aug-17	4.32	88.60	7.08	29.28
14-Sep-17	9.98	84.01	6.01	27.67

Table 5. DHP PAI

Acquisition Date	PAIeff	PAItrue	Q1 PAI	Q2 PAI	Q3 PAI	Q4 PAI	Clumping Index
27-Apr-17	3.55	6.13	7.07	5.91	6.16	5.73	0.58
26-Jun-17	3.80	6.45	8.27	7.11	5.96	5.66	0.59
25-Jul-17	4.14	6.53	7.66	6.68	6.67	6.62	0.63
9-Aug-17	4.48	6.99	6.72	6.59	7.23	6.79	0.64
14-Sep-17	3.83	6.51	7.17	7.25	6.79	7.46	0.59

DHP PAI (PAItrue) results showed a distinct phenology (Figure 3), particularly when comparing the April acquisition to the August acquisition. August PAI results showed a particularly large jump in PAI compared to June and July; post-harvest results more closely matched those in June and July than August. A total difference of 0.86 PAItrue occurred between leaf-off and peak leaf-on acquisition. Post-harvest results then dropped down 0.48 PAItrue from peak acquisition PAI. Post-harvest PAI in September was 0.38 higher than the leaf-off PAI. The high leaf-off PAI and low relative difference (14 percent increase in PAI from leaf-off to leaf-on) is due to the coniferous species, which comprised 63 percent of the basal area in the plot (Table 1). Quadrant values in general showed less of a seasonal pattern and varied with more error.

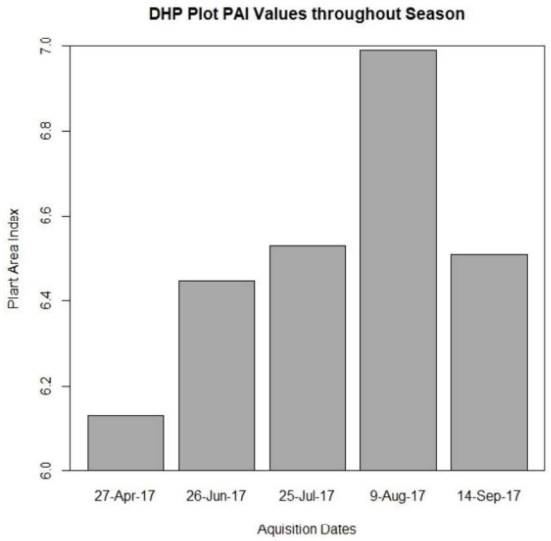

Figure 2. DHP PAI. DHP PAI values of entire plot throughout acquisition dates. Shows the difference between leaf-off and leaf-on PAI and the sharp decrease caused by harvesting.

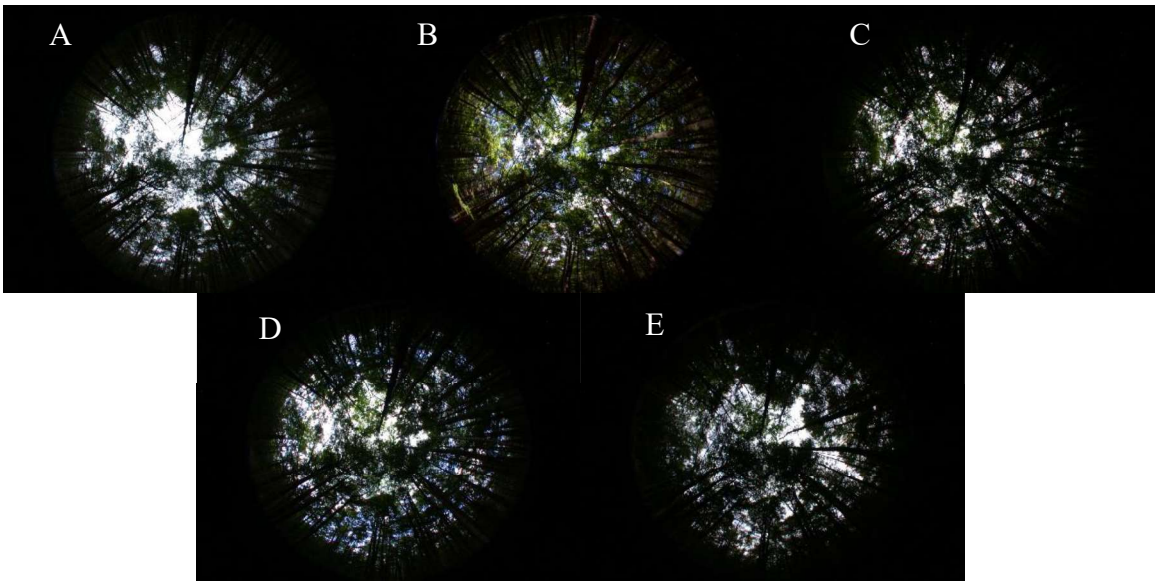

Figure 3. DHP Series. Changes throughout the season can be seen in the hemispherical images. All of these images are taken from position (6,6) in the plot. A: Taken in April, this image is from leaf-off conditions. B: Taken in June, this image shows a much denser canopy than A and is slightly overexposed. C: Taken in July, this image was taken on a day with ideal sky conditions and shows strong contrast between vegetation and sky. D: Taken in August just before destructive harvesting. E: Taken in September post-harvest, trees are shown to be absent in this image due to the harvesting activity leading to more sky pixels present and more gaps in the canopy.

The PAI values shown in Figure 2 are PAItrue values modeled using the clumping index output given directly from CAN-EYE. These values and PAIeff values are dependent on the classification of the images, which is done by the user from image interpretation and color. Classification may be affected if image exposure is not properly set (Figure 4). Weather and sky conditions may have large effects on results from DHP as well (Jonckheere et al., 2004 and Woodgate et al., 2016). Alternative methods of acquiring PAI or LAI used here, i.e., TLS or harvesting with destructive sampling, are less dependent on the user experience or sky conditions at the time.

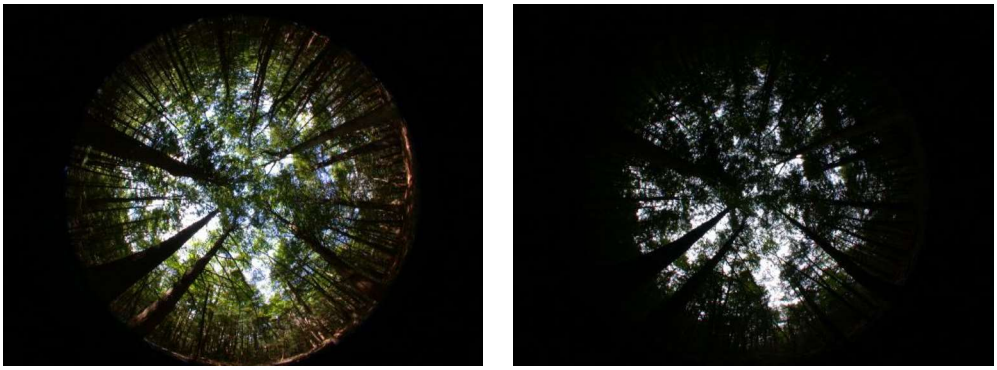

Figure 4. DHP Differences. The image on the left was taken on a day with frequently changing sky conditions and is overexposed leading to large color variations between different vegetation in the image. The image on the right was taken on a day with more universal cloud cover and has the proper exposure to differentiate between sky and vegetation pixels, leading to a better classification.

TLS

TLS acquisitions were processed to give effective PAI values as well as a Plant Area Volume Density (PAVD) profile (Appendix Figure 17) for the whole plot and individual scan sites. This processing was done by Dr. Kim Calders at the Ghent University. Whole plot results compare favorably to DHP results on the two matching acquisition dates (Table 6 and Figure 5). TLS results were slightly higher than whole plot DHP results and are well within expected values. This agreement between the two optical methods validates the PAI values retrieved from DHP, considering that TLS data are unaffected by sky conditions and user interpretation.

Table 6. TLS PAI

Acquisition Conditions	DHP PAIeff	TLS PAIeff
Leaf-off	3.55	3.62
Leaf-on	4.48	4.52

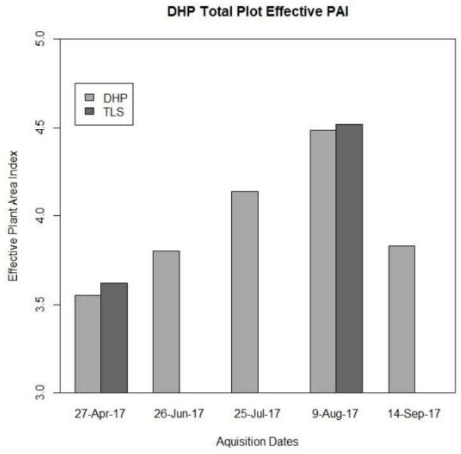

Figure 5. DHP and TLS PAI

Destructive Sampling

Leaves and Twigs

Final leaf and twigs measurements were taken and processed to give a twenty-tree sample of the stand. Leaf and twig samples from single trees within five size classes for each of four species were acquired (Table 7). Samples from trees in size class 4 were taken from the adjacent North Plot, while the remaining 16 samples were acquired from the Main Plot (Figure 6).

Table 7. Sampled Leaves and Twigs

		Leaf		Twig	
Size class	DBH, cm	Weight, kg	Area, m^2	Weight, kg	Area, m^2
		Eastern hemlock			
1	7.8	0.2919	2.5225	2.7261	4.1627
2	18.9	5.6035	48.4159	15.1770	23.1753
3	23.7	5.1887	45.1902	6.1778	9.4335
4	34.5	18.5170	163.1749	14.9881	22.8869
5	40.6	14.8534	124.7586	10.2334	15.6263
		White pine			
1	13.9	1.3121	15.2443	0.8834	0.9784
2	21.5	1.9618	15.4040	3.8819	4.2992
3	25.4	4.4241	36.3530	1.5953	1.7668
4	33.3	12.8373	106.1209	13.0468	14.4493
5	41.3	14.5726	117.9137	1.7634	1.9530
		Red maple			
1	8.1	0.4549	9.7397	0.0215	0.0208
2	11.3	0.7981	15.4905	0.0283	0.0274
3	12.9	1.3291	26.7334	0.0503	0.0487
4	21.8	4.2447	51.9695	0.4011	0.3883
5	22.1	4.4223	80.9041	0.2706	0.2619
		Red oak			
1	19.6	2.2094	26.7894	0.0182	0.0118
2	26.8	6.7628	76.5499	0.8342	0.5420
3	32.8	7.0786	77.5370	0.7316	0.4753
4	36.3	4.0344	51.1444	0.5101	0.3314
5	50.1	11.7866	154.3297	1.8212	1.1832

Table 8 (p. 34) shows leaf and twig areas, as well as specific leaf and twig areas, by species. Specific leaf areas varied over the four species, with the deciduous species having higher specific leaf areas than the coniferous. Red maple overall had the highest SLA at 182.94 $cm^2\ g^{-1}$, while eastern hemlock had the lowest SLA at an average of 86.40 $cm^2\ g^{-1}$. This contrasted with specific twig areas where eastern hemlock had the highest average STA of 15.27 $cm^2\ g^{-1}$ and red oak had the lowest average STA of 6.50 $cm^2\ g^{-1}$.

These differences have an impact on the leaf-twig ratios of the species, driving down eastern hemlock and white pine ratios and driving up red maple and red oak ratios. Overall this means that hemlock in the plot has a higher presence of fine branches per each unit of leaves. Note that individual SLA values were computed for each tree while

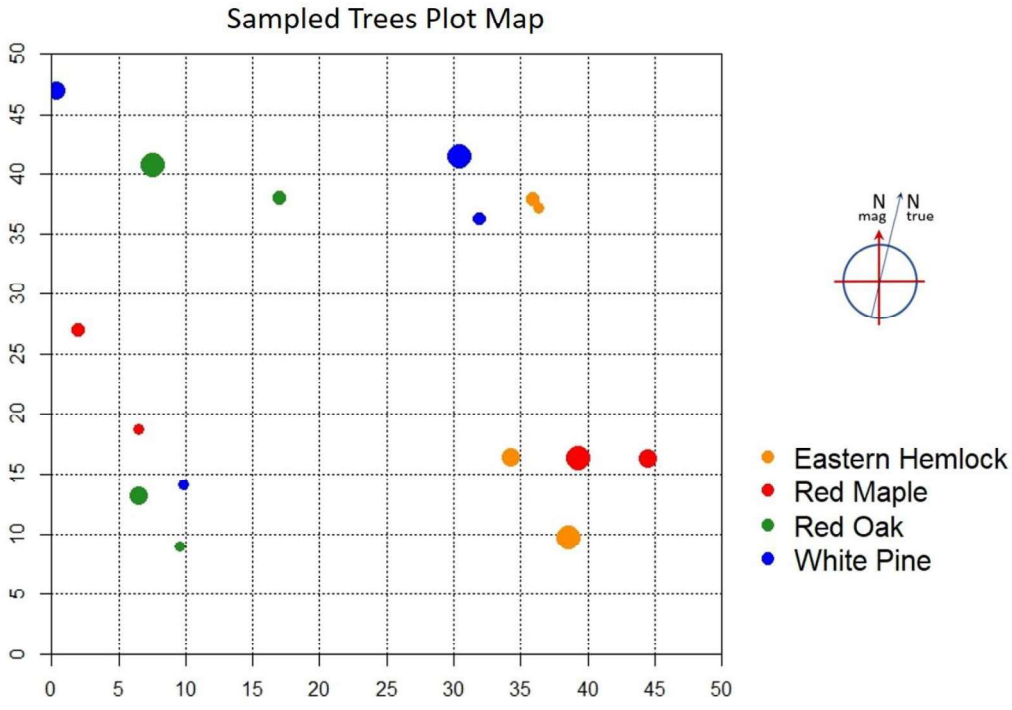

Figure 6. Sampled Tree Map. The sixteen sampled trees from the main plot locations and sizes are represented in this map.

STA values were averaged over the whole species in order to calculate the total leaf area of each sample tree. This was done due to the small sample size of STA values for sample trees.

Allometries

Species-specific allometric equations were developed to fit the sample data for leaves and twigs using the basal area and leaf or twig area of trees (see pp. 25-26). Coefficients of the models can be seen in Table 8. Results varied for each species, with the lowest standard error in red maple estimates and the highest standard error in white pine. Figure 7 shows the data points for each species, curves fitted from the equations, and 1-standard error upper and lower bounds. The calculated total one-sided leaf area in the plot is 14,948.29 m^2 with bounds of 10,396.99 m^2 and 21,518.26 m^2.

These errors are due to the variance in fitting allometric models to a small number of sample data points. While the confidence in the destructive sampling measurements is high, the confidence in the total plot leaf area using these allometric models needs to be constrained by possible errors. These errors become larger as basal area increases, leading to the largest errors in mature trees. However, large trees are rare in this plot as 75 percent of trees fall below 750 cm^2 basal area.

Table 8. Allometric Equation Plot Results

Species	Stems	Total area, m^2		Leaf-twig ratio	Specific areas, cm^2g^{-1}		Regression coefficients			
							Leaf		Twig	
		Leaf	Twig	*R*	Leaf	Twig	a	b	*a*	*b*
Eastern hemlock	152	10159	1906.75	5.328	86.403	15.270	8.527	0.796	9.227	0.428
White pine	8	879	34.620	25.380	88.090	11.075	6.354	1.051	6.824	0.554
Red maple	50	1811	6.942	260.876	182.94	9.682	8.688	0.757	0.873	1.137
Red oak	32	2099	14.955	140.354	120.34	6.497	8.275	0.771	-6.233	12.120
Total, plot	242	14948	1963.27							

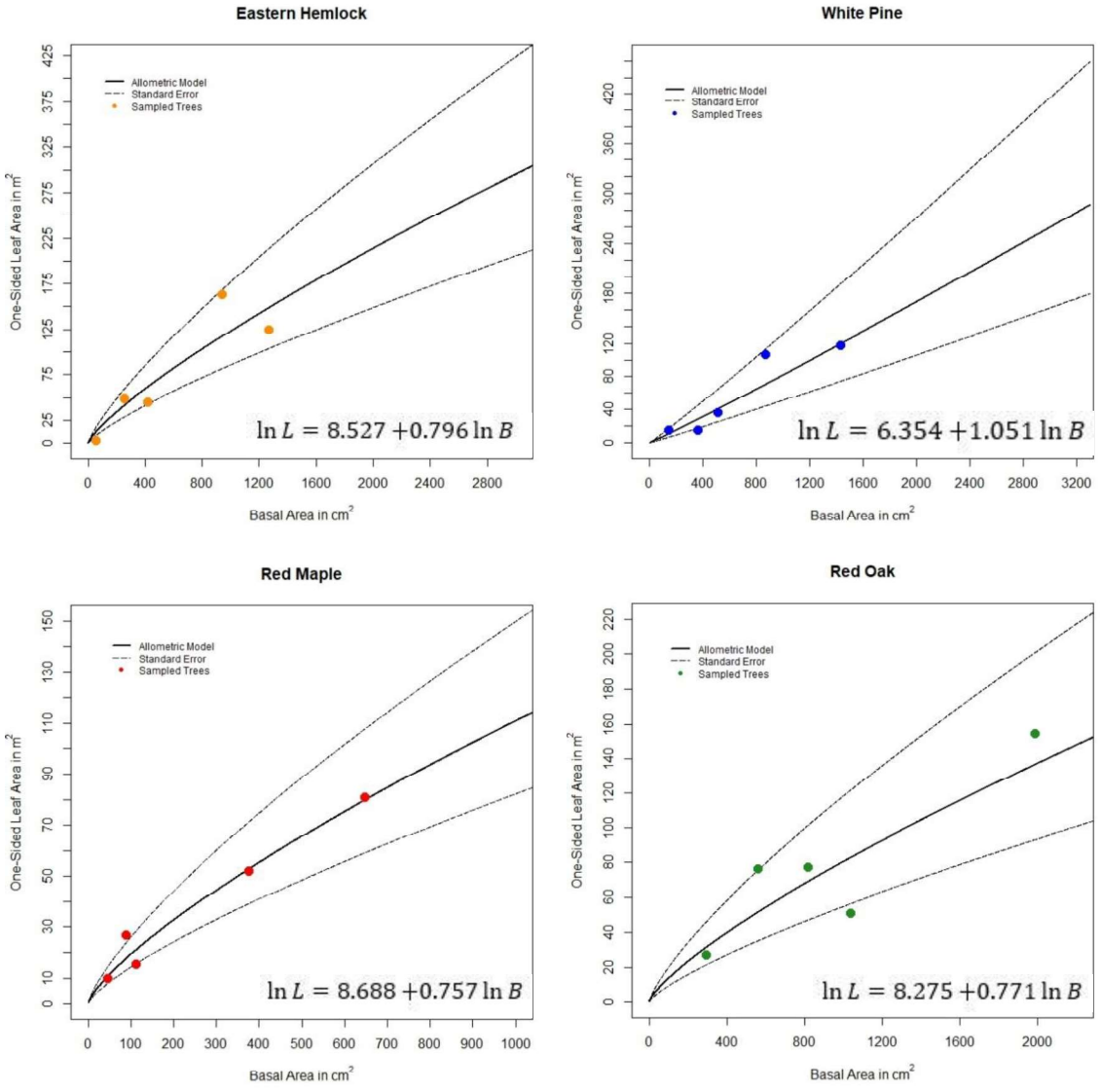

Figure 7. Leaf Allometry. Curves of the allometric leaf area models with standard errors and sampled trees shown.

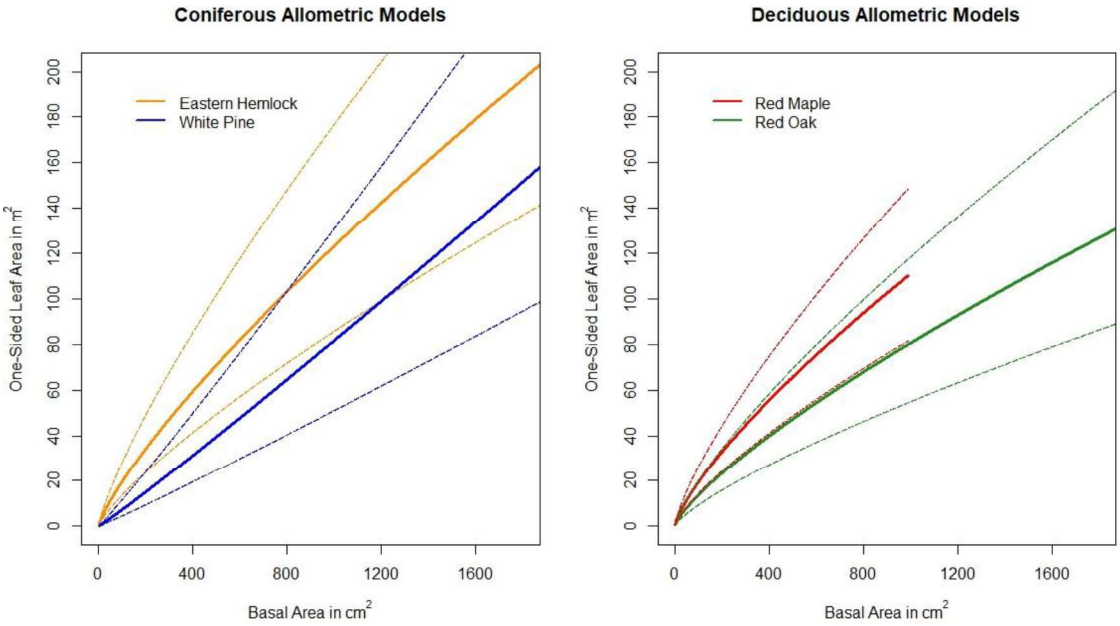

Figure 8. Leaf Allometry Comparison. Curves of the allometric leaf area models with standard errors scaled to the same ranges to better compare the models.

The twig area allometric equations showed higher variance than those developed for leaves. Both standard errors and p-values were larger. This could be due to higher variability in twig composition of a tree than leaf composition. More samples would have aided in lowering errors of the twig area models, but the final results aren't altered drastically within the standard errors, and taking more destructive samples is costly.

Table 9. Allometric Equation Errors

	Leaf Allometry		Twig Allometry	
Species	Standard error	p-value	Standard error	p-value
Eastern hemlock	0.3616	0.1078	0.5522	0.1451
White pine	0.4707	0.0307	1.0640	0.4342
Red maple	0.3001	0.0119	0.5787	0.0236
Red oak	0.3840	0.0646	1.1120	0.0728

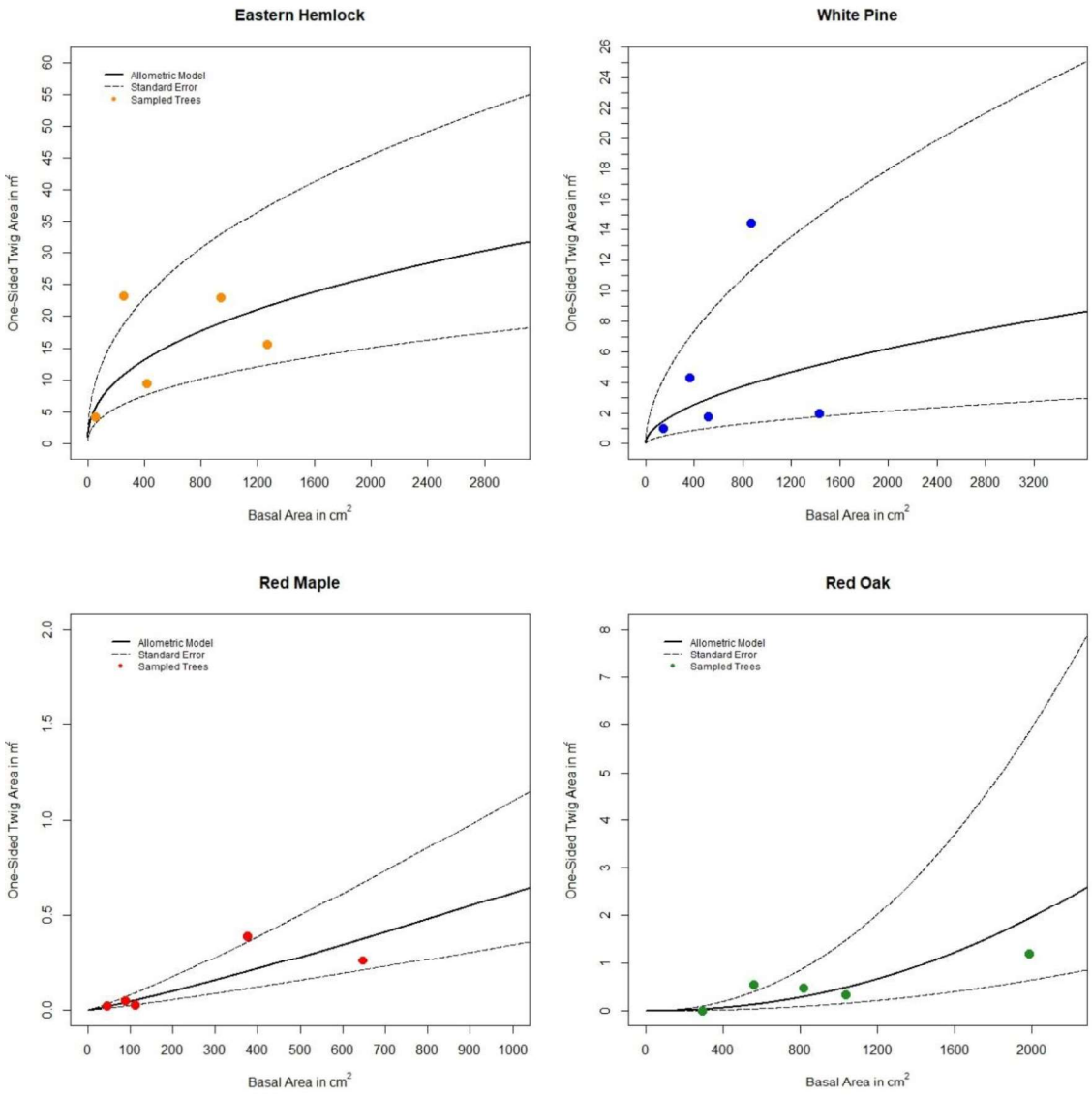

Figure 9. Twig Allometry. Curves of the allometric twig area models with standard errors and sampled trees shown.

The white pine twig area model performs poorly, with a p-value of 0.4342. The point from class 4 is quite high, and could be regarded as an outlier. However, given the small number of points, it was retained in the fitting. In general, twig areas of the coniferous trees were much higher, given size class, than those of the deciduous trees

(Table 7) (Figure 10). This is due to a combination of the larger STA values and much more twig mass overall, particularly in the hemlocks.

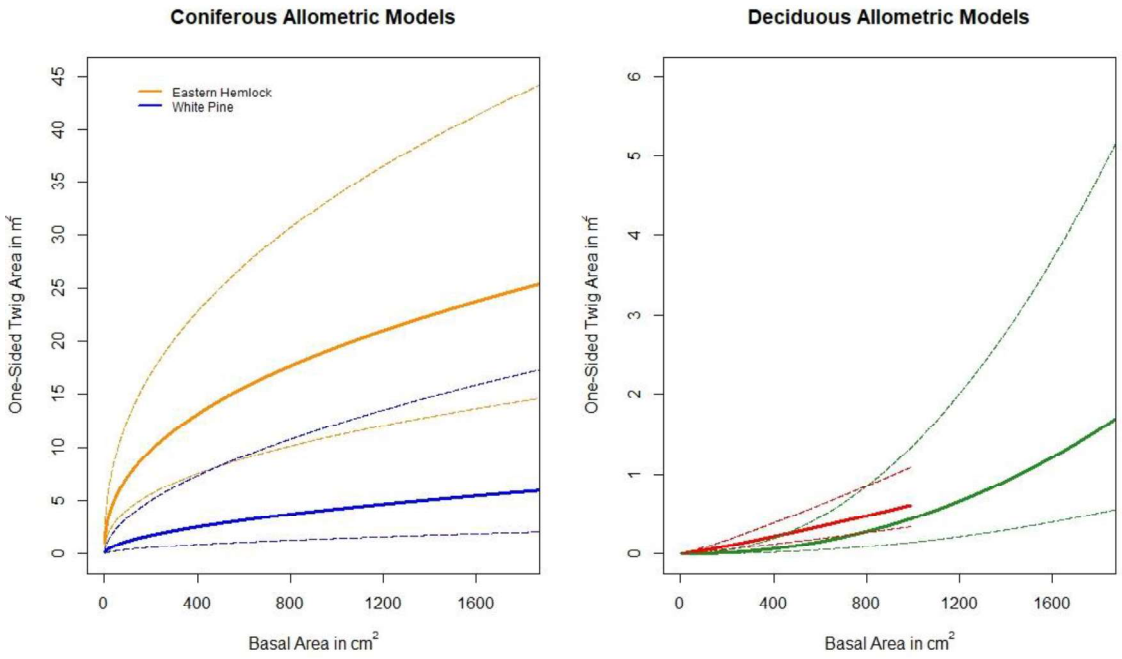

Figure 10. Twig Allometry Comparison. Curves of the allometric twig area models with standard errors scaled to the same basal areas to better compare the models. The twig areas for the coniferous trees are much larger than those of the deciduous.

LAI from Destructive Sampling and Hemispherical Photography

Leaf Area Results

Combining the species-specific allometric equations for leaf area as a function of stem basal area with the census of trees in the main plot at the time of harvest provides an LAI of the main plot as 5.98 (4.16-8.61), composed of a coniferous LAI of 4.42 and a deciduous LAI of 1.56 (Table 11). Coniferous leaf area dominated, with 68 percent of the total leaf area alone provided by eastern hemlock (Table 10). An after-harvest tree census, omitting trees felled for the destructive sampling effort, provides a total LAI of

5.08, with coniferous and deciduous leaf areas of 3.73 and 1.34 respectively. The loss in leaf area during the harvesting process is then 0.90 units.

Table 10. Species LAI Contribution

	Eastern Hemlock	White Pine	Red Maple	Red Oak
Pre-Harvest	4.06 (2.83-5.83)	0.35 (0.22-0.56)	0.72 (0.54-0.98)	0.84 (0.57-1.23)
Post-Harvest	3.45 (2.41-4.97)	0.27 (0.18-0.44)	0.63 (0.47-0.85)	0.71 (0.49-1.05)

To compare with these values, we have DHP PAI values acquired before (August 9) and after harvest (September 14), as well as a DHP PAI estimate from 27 April, before leaf-out of the deciduous species (i.e., leaf-off conditions). To estimate the LAI at that time from destructive sampling, we will assume that the coniferous LAI is the same in April and August. That is, new conifer leaf growth has replaced old growth shed from prior years in equal measure. With deciduous LAI at zero, the leaf-off LAI from DS is therefore 4.42 (Table 11).

Table 11 also shows PAI values estimated with DHP before and after harvest. Before comparing these to the LAI values, we note that the PAI is composed of both leaf and wood area indexes (WAI). Thus, if PAI is to estimate LAI, WAI must also be derived. For leaf-off and leaf-on conditions,

$$PAI\_leaf\text{-}off = WAI + LAI\_conif$$

$$PAI\_leaf\text{-}on = WAI + LAI\_decid + LAI\_conif$$

and

$$WAI = PAI\_leaf\text{-}off - LAI\_conif$$

$$WAI = PAI\_leaf\text{-}on - LAI\_decid - LAI\_conif$$

Note that in the simpler case of a fully-deciduous forest, WAI = PAI_leaf-off (Woodgate et al., 2016, Calders et al., 2018). In our case however, WAI = PAI_leaf-off – LAI_conif. Assuming as above that LAI_conif is unchanged, we have WAI = 6.13 – 4.42 = 1.71 (Table 11). We may also derive WAI for leaf-on conditions as WAI = 6.99 – 4.42 –1.56 = 1.01.

In theory, these values should match, as the woody component will only change slowly. To introduce this constraint, we will use a single clumping index in the estimation of PAI from effective PAI. This assumption is also supported by Woodgate et al. (2016) on the basis of simulations of leaf-off and leaf-on forest images and TLS scans. CAN-EYE provided clumping indexes of 0.58 for leaf-off conditions and 0.64 for leaf-on. Using the leaf-off value for leaf-on conditions, derived PAI increases from 6.99 to 7.72 (Table 11) and WAI_leaf-on becomes 1.74, which is very close to WAI_leaf-off. If this clumping value is used to estimate PAI from TLS values for effective PAI (Table 6), both PAI and WAI are very close to DHP values, which also supports the clumping value choice. In addition, the revised values generate an estimated deciduous LAI (1.59) very close to that observed by DS (1.56).

The above analysis shows that WAI, as the difference between two larger quantities, is quite sensitive to small changes in the clumping index. Thus, it is important to understand and obtain confidence in the algorithms that estimate the clumping index from the spatial and geometric pattern of angular gaps within and between tree canopies. CAN-EYE's complex method takes full advantage of radiative transfer theory and simulation, thus providing a degree of confidence, but other methods could be tested.

Although some simulations of WAI have validated DHP retrievals (Woodgate et al., 2016), actual measurements of WAI are generally lacking. However, the destructive sampling carried out as part of the Harvard Forest RCN Calibration Activity may provide the opportunity to estimate woody surface area of the destructively sampled trees. Another approach would be to use quantitative structure models derived from TLS, which would provide surface areas derived from scans of the DS trees as well as other trees in the stand (Raumonen et al., 2013, Calders et al., 2015). These independent checks would be quite helpful and will be pursued in the future.

Calders et al. Regression Formula

A separate way to calculate PAIeff, and given a clumping index, PAItrue, is to use the model developed with simulation and real TLS data by Calders et al. (2018). Their linear model relates effective LAIeff to effective PAI corrected for effective WAI:

$$eLAI = 0.552 + 1.069(ePAI - eWAI)$$

Applying TLS and DS values from Table 6 and Table 11, effective LAI is 4.26, and when adjusted for clumping with a clumping index of 0.58, a PAItrue value of 7.34 is obtained. This value is within five percent of the clumping-corrected DHP PAI and using the methods above provides a WAI of 1.74. This further verifies the accuracy of the DHP PAI, the allometric LAI, and the calculated WAI results.

Table 11. LAI Results

Acquisition Date	Allometric LAI	Coniferous Allometric LAI	Deciduous Allometric LAI	DHP PAI	Clumping DHP PAI	TLS PAI	WAI
27-Apr-17	4.42 (3.05-6.39)	4.42 (3.05-6.39)	0	6.13	6.13	6.24	1.71
9-Aug-17	5.98 (4.16-8.61)	4.42 (3.05-6.39)	1.56 (0.79-1.80)	6.99	7.72	7.79	1.74
14-Sep-17	5.08 (3.54-7.31)	3.73 (2.58-5.41_	1.34 (0.95-1.90)	6.51	6.49		1.42

Table 11. LAI Results. Calculated and modelled LAI, PAI, and WAI values are found in this table. TLS PAI values are calculated from TLS PAIeff values by applying a 0.58 clumping index that was calculated from leaf-off DHP. The Clumping DHP PAI value varies from the DHP PAI column in that the same clumping index of 0.58 was applied to the DHP PAIeff results for all dates as opposed to individual date calculated clumping index values. This gave a closer match in WAI, validating the results.

Post-Harvest Plant and Leaf Area Changes

Post-harvest WAI was determined similarly for DHP data, giving a clumping-corrected DHP PAI value of 6.49, a WAI of 1.42, and a Calders et al. (2018) modeled PAI of 6.37. The total change in PAI following harvest, after correcting for clumping, is 1.23, a decrease of 16.84 percent. The total change in photosynthetically active material in the forest due to harvest was 0.90 LAI, with an absolute maximum difference of 5.07 LAI when taking using the maximum probable LAI in August and the minimum probable LAI in September, although a difference this great is highly unlikely. Total vegetation area index comparisons and validated results are visualized for pre- and post-harvest in Figure 11 and Figure 12.

Species-specific contributions to LAI (Table 11 and Figure 13) show the dominance of eastern hemlock in the plot. The error in the allometric calculations of hemlock is greater than the next most dominant species total LAI. In similar plots that are dominated by single species, it may be advantageous to take more samples of the dominant species to reduce errors. For example, it may have been more helpful to

constrain errors in the allometric LAI estimate in this plot to sample more than five eastern hemlocks in place of focusing on the low count white pine. As it stands now, each species was treated with equal importance to the plot in the sampling scheme. This sampling scheme emphasized developing an understanding of the four species overall, in place of simply understanding the one 50 by 50-m plot.

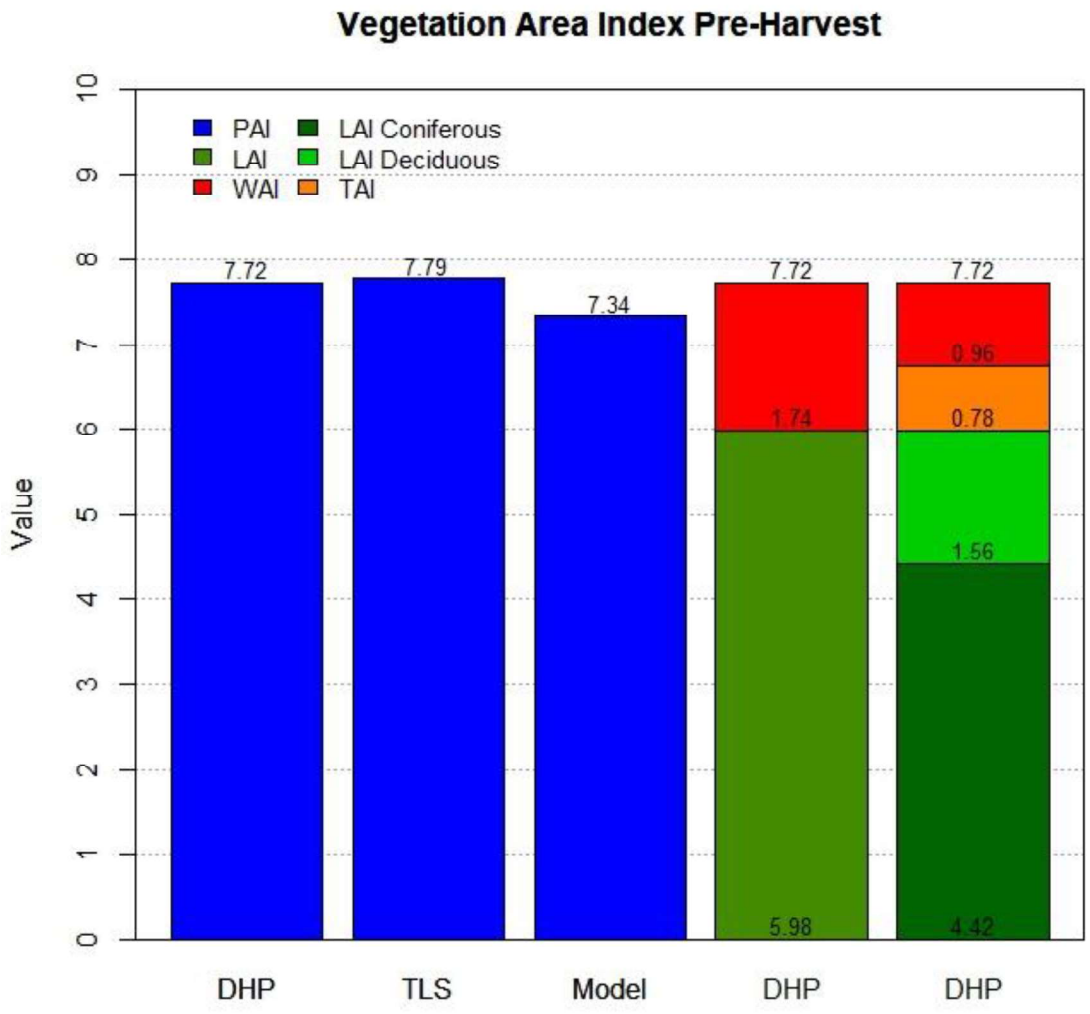

Figure 11. VAI Prior to Harvest

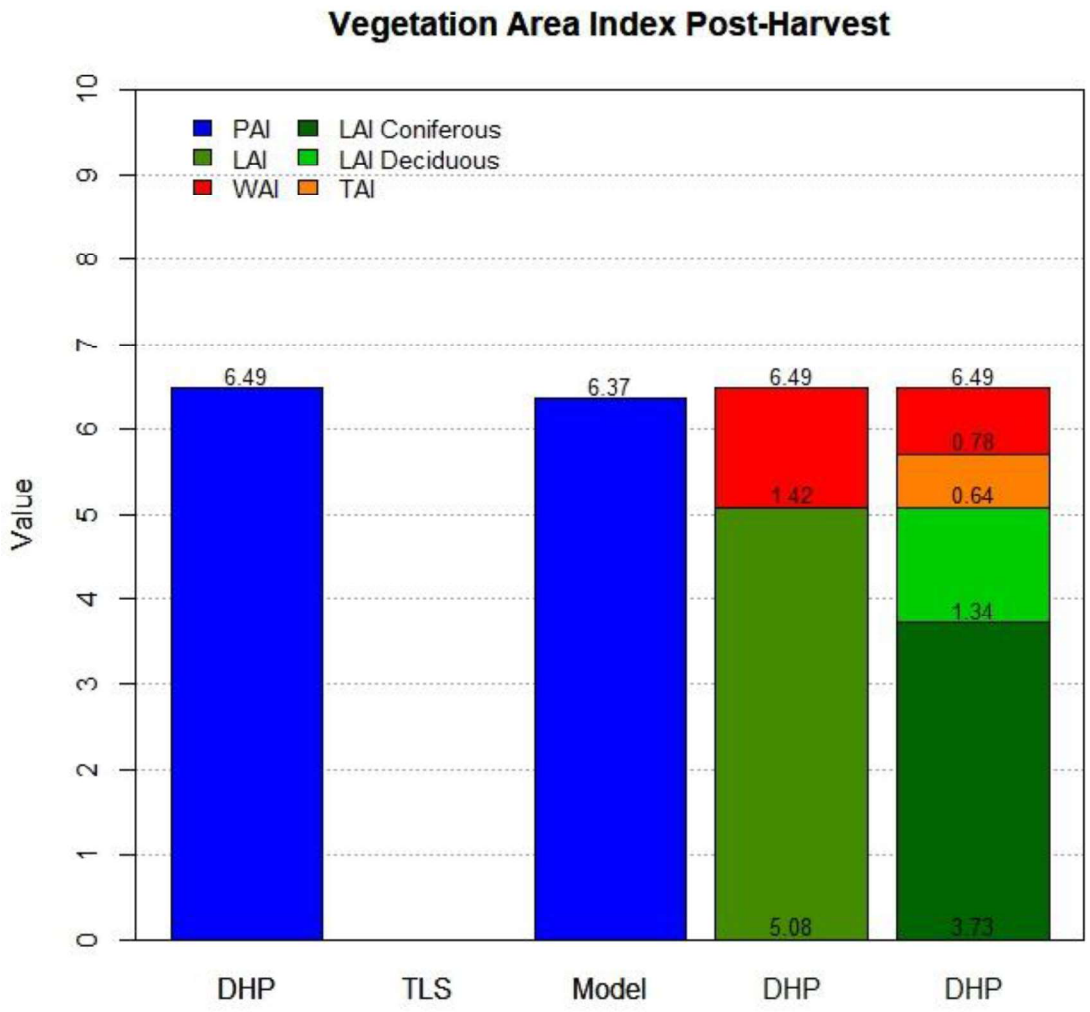

Figure 12. VAI Post-Harvest

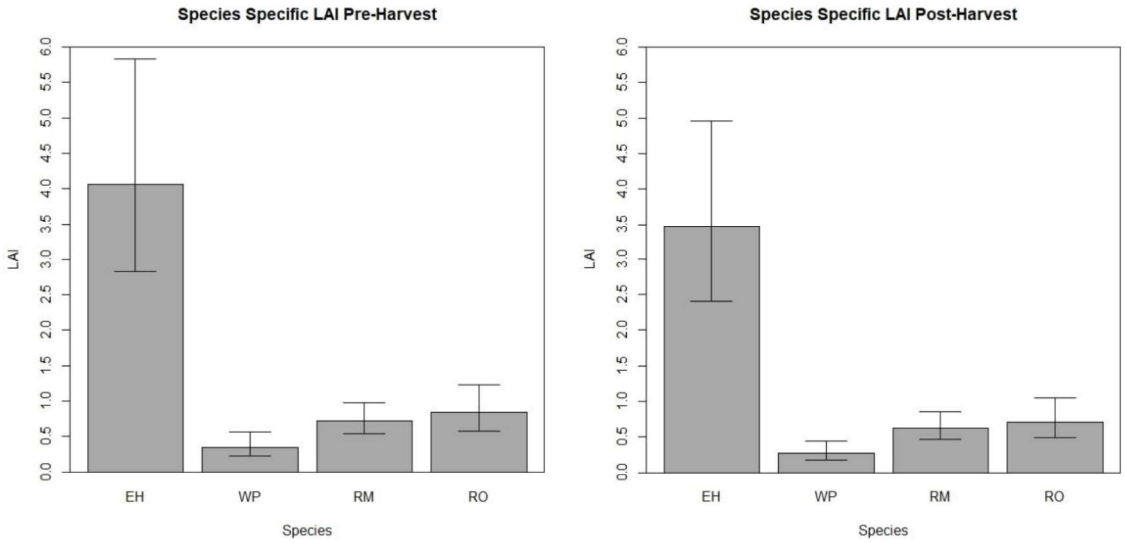

Figure 13. Species LAI Contribution. LAI values are shown with standard errors. Eastern hemlock contributes the vast amount of LAI to the plot when compared with the other three dominant species.

Twig Area Results

Total TAI from the destructive sampling and developed allometric equations is estimated at 0.79 with a standard error range of 0.45 to 1.39 (Table 12). This value was dominated by hemlock, with 0.76 TAI, or 96.2 percent of the total twig area (Table 13 and Figure 14). The dominance arises because the STA for eastern hemlock is significantly higher than that of the other species and eastern hemlock dominates the plot (Table 7). After harvest, total TAI dropped by 0.15 to 0.64.

To verify the allometric TAI values, TAI was calculated as described in Section 2.1.6. A ratio value, *R*, of 12.43 was calculated by the total leaves per twigs of the sampled trees. The ratio was then used to calculate a TAI of 0.56 for pre-harvest and 0.47 for post-harvest conditions. These values lie within the standard error for the allometric results, but are comparatively lower (Figure 15).

Assuming true TAI values lie between the calculated and allometric values of 0.56 and 0.79 pre-harvest and 0.47 and 0.64 post-harvest, TAI accounts for approximately 32 to 45 percent of WAI pre-harvest and 33 to 37 percent of WAI post-harvest. TAI is found in the within-crown clumping of DHP PAI and is a part of the WAI. Estimating TAI directly from destructive sampling and allometric equations helps to better constrain estimates of WAI and understand where the woody area comes into account. Using these data, the pre-harvest DHP PAI value of 7.72 that has already been corrected for between-crown clumping can be reduced by 0.56 to 0.79 due to within-crown clumping of TAI.

Table 12 TAI Results. TAI results from allometries and calculated using R

Acquisition Date	Allometric TAI	Calculated TAI
27-Apr-17	0.79 *(0.45-1.39)*	
9-Aug-17	0.79 *(0.45-1.39)*	0.56
14-Sep-17	0.64 *(0.36-1.12)*	0.47

Table 13. Species TAI Contribution

	Eastern Hemlock	White Pine	Red Maple	Red Oak
Pre-Harvest	0.76 (0.44-1.32)	0.01 (0.005-0.04)	0.002 (0.001-0.005)	0.006 (0.002-0.02)
Post-Harvest	0.62 (0.35-1.08)	0.01 (0.003-0.03)	0.002 (0.001-0.004)	0.005 (0.002-0.02)

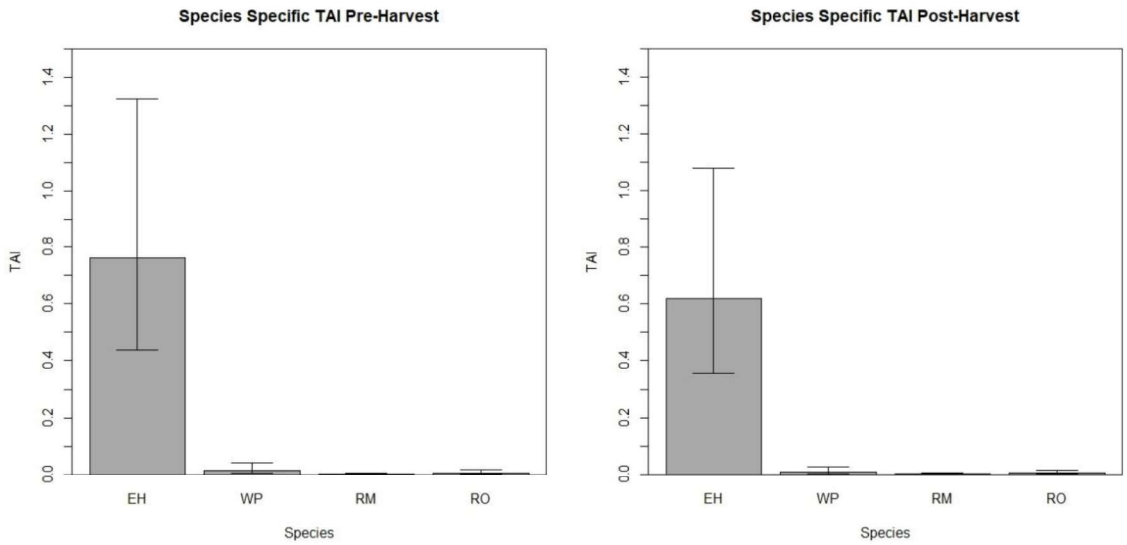

Figure 14. Species TAI Contribution. Species TAI values are shown with standard errors. White pine, red maple, and red oak have a much smaller contribution to the total plot TAI when eastern hemlock error is taken into consideration.

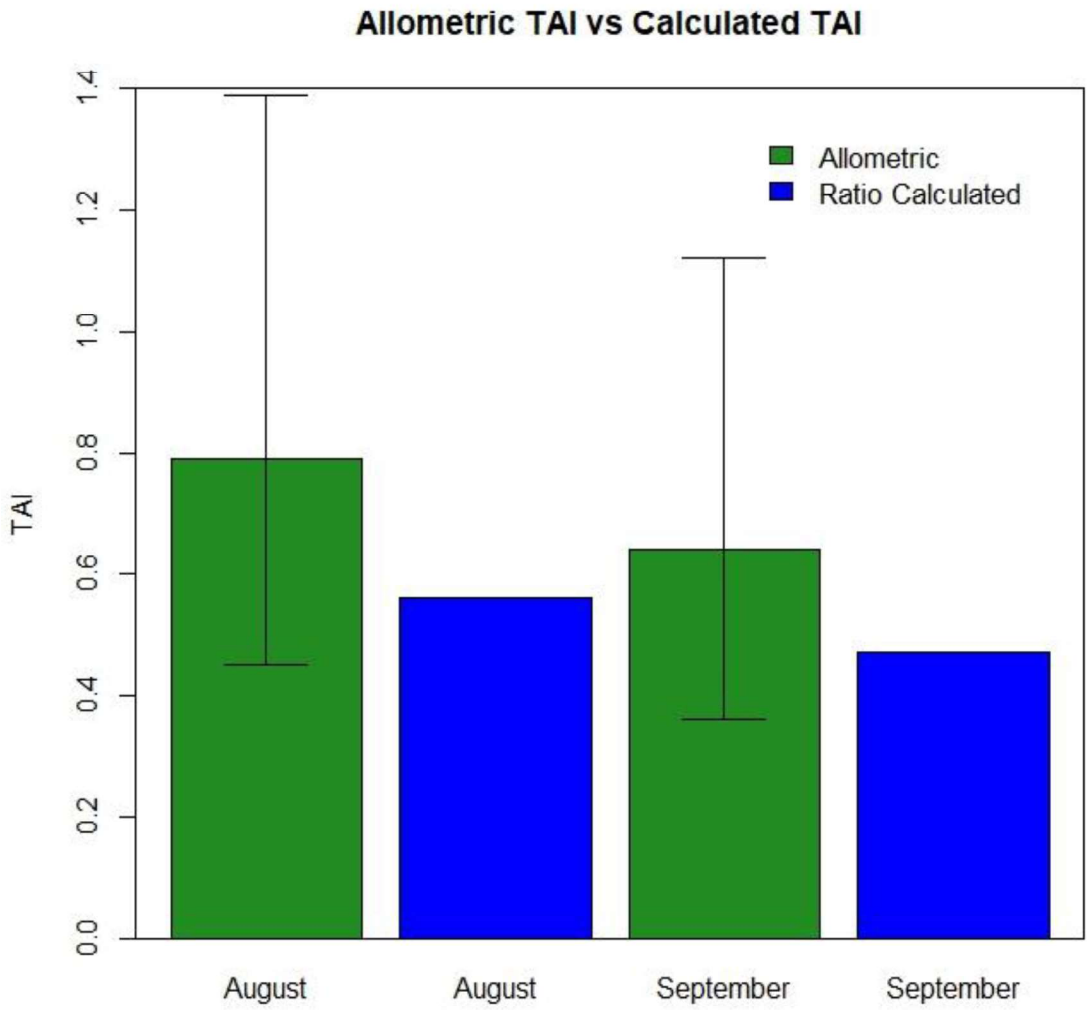

Figure 15. TAI Differences. Differences in the allometric equation TAI and the TAI calculated using an *R* of 12.34. Values can be seen in Table 12.

DISCUSSION

Ecological Impacts

LAI is one of the essential climate variables identified by the Global Climate Observing System (GCOS). It is a key parameter for various applications in hydrological, ecological, and biogeochemical models. Many global LAI products have become available since the early 2000s (Fang et al., 2014). While these global LAI products are essential in driving future ecological models, plot level LAI measurement is needed for validation of large-scale and satellite remote sensing LAI applications.

Many indirect, remote sensing methods estimate PAI, not a true LAI (Jonckheere et al., 2004). Photosynthetically active leaves and woody material perform different functions for trees and a forest as a whole, which emphasizes the importance of separating PAI into WAI and LAI. Our study found the LAI of a 50 x 50-m plot using destructive methods. From there, PAI found by optical methods using TLS and DHP was separated into LAI, WAI, and TAI. This gave a richer and more accurate understanding of the structure of the forest.

A twig-leaf ratio, *R*, was developed for four species, *Tsuga canadensis*, *Pinus strobus*, *Quercus rubra*, *Acer rubrum*, and the plot as a whole. While separating large trunks and branches from leaves in DHP and TLS data is daunting, it has been performed (Li et al., 2013, Woodgate et al., 2016 and Calders et al., 2018). It is more difficult to separate the twig area from leaf areas that are typically retrieved. This TAI was shown to be a significant portion of the WAI in eastern hemlock-dominated forests, and may be a part that is missed in separating LAI and WAI within optically-derived PAI. Using an *R*

value can help in separation of leaves and twigs in mixed temperate forests with similar species composition, allowing for further accuracy in LAI estimation with indirect methods.

The sampling method in this plot was similar in nature to selective logging. Selective logging is a method used as a compromise between socioeconomics and environmental costs. Environmental costs are supposedly mitigated through reduced impact logging practices (Medjibe et al., 2011). Martin et al. (2015) found little difference in reduced impact logging methods and conventional selective logging methods when it came to impact on post-logging biomass. Their findings suggest that intensity, not logging method, is the main factor of post-logging species richness and carbon emissions related to logging.

Many non-target trees are damaged near and adjacent to the trees targeted for harvest, and frequently these trees are felled and become a carbon source contributing to higher respiration rates. In this study, the sampled trees are synonymous with the trees targeted for harvest. To make room for sampling and to take down the 16 sample trees in the Main Plot and 4 trees in the North Plot, 31 additional live trees were felled in the plot. Total LAI lost from the plot due to the felling of sampled trees was 0.34. Total LAI lost due to the activity as a whole was 0.90, yielding a difference of 0.56 LAI in collateral loss. This loss of LAI contributes to a loss in GPP due to a loss of photosynthetically active material and an increase in respiration, leading to an even greater decrease in NPP.

It is important to note that LAI is only a small portion of forest structure that contributes to carbon cycling of forest ecosystems. Function as well as structure of the

forest is key in understanding the drivers of NPP and possible source-sink capabilities of a forest stand. Water availability, nitrogen concentration, tropospheric ozone presence, soil type, and root structure and health are just a few examples of complex elements beyond LAI that are essential in understanding the status of a forest as a source or sink of CO_2 (Templer 2013 and Templer and Reinmann, 2011).

Methods and Sources of Error

Estimations of DHP PAI can be adversely affected by camera exposure, sky conditions, and classification accuracy. To reduce error due to camera over- or underexposure, camera exposure was determined by light meter and was bracketed by ±1 *f*-stop (p. 19). Images were acquired on dates with mostly uniform overcast sky to prevent issues of sky differences affecting the estimation of gap probability with zenith angle. Classification accuracy was limited by sample selection in CAN-EYE and masking of areas in images, such as non-forest elements and bright, highly reflective tree trunks, that may have given RGB-based classification issues. Classification of sky and vegetation pixels was performed by a single individual to provide consistency. Use of a single operator is an attempt to limit errors, as Hancock et al. (2014) found that manual classification through thresholding differed by as much as 17 percent when performed by different operators. In future analyses, methods of using automated thresholding could possibly help further limit human error in DHP PAI results (Jonckheere et al., 2005). The DHP PAI results therefore need to be understood as an estimation of the forest. However, as DHP estimation techniques have evolved over time, limiting of errors has improved

significantly and results now typically match favorably with destructive methods (Jonckheere et al., 2003, Fang et al., 2014).

Estimations of DHP PAI in this study closely matched PAI in a study performed in the Harvard Forest and two other similar New England forests by Zhao et al. (2011). When the same clumping index used in the study plot is applied to PAIeff values from Zhao et al. (2011), their data show a PAI in the range of 5.91-9.05. The value found in this study of the leaf-on, pre-harvest plot of 7.72 falls in the middle of these bounds. TLS PAIeff values also closely match DHP values found in this study, giving confidence in both results. The model developed by Calders et al. (2018) also gives PAI results similar to DHP and TLS, further validating those PAI methods in this plot.

Total leaf and twig weights were gathered directly from sampled trees with only small errors, likely due to leaves and twigs lost during felling. Therefore, the results of leaf weights are not regarded as a significant source of error in this study. Total tree leaf area was calculated using SLA values developed according to Section 2.1.6. Nine samples were taken from each tree, stratified by lower, middle, and upper canopy height. Weights and areas of these samples were taken to determine SLA values. Weight and area are directly measured with three-digit precision and are therefore not regarded as a source of error in the analysis. Mean SLA values for each tree were then applied to the total tree leaf weights to find the total one-sided leaf area of each sample tree. STA values and total projected twig areas were found similarly; however, the STA samples were taken throughout the canopy where available as destruction proceeded, rather in nine distinct samples.

The total projected leaf and twig areas of the twenty sampled trees are well constrained and understood. The allometric models developed from these samples, however, are where possible errors in the plot LAI estimations come in to effect. The allometric models developed for the four species for both projected leaf and twig area estimation by basal area have standard errors associated with them that are seen in Figure 7 and Figure 9. Due to the logarithmic regression function, these values increase as basal area increases, particularly in projected twig area estimation. These large ranges most likely represent individual variation in trees within size classes, and could be mitigated by adding samples although at high cost. It is important to note, however, that over 75 percent of the individual tree basal areas in the plot fall below 750 cm^2, and in this range, error bounds tend to be tighter.

When errors in individual tree leaf areas are extended to the sum of leaf areas for the total plot, they generate a range of 4.45 (4.16–8.61) total LAI pre-harvest and 3.77 (3.51–7.31) LAI post-harvest around estimated values of 5.98 and 5.08 LAI respectively. Khomik et al. (2014) performed a study in the Harvard Forest looking at a regenerating clearcut environment. They used similar methods of looking at individual tree SLA to determine leaf area of the whole plot. Their estimated LAI values of 2.5±0.4, 2.2±0.2, and 2.9±0.2 fall short of the bounds in this study but the authors explain an expected LAI of around 5.0–5.5 after regrowth is complete by pointing to studies done by Boring et al. (1981) and Marks (1974). These values would fall near the value of 5.98 found in the study plot, helping give confidence in the LAI found by our allometry. Song and Dickinson (2008) worked in a similar forest composition and found LAI results near

those in this study by using allometric equations developed from crown diameter in place of basal diameter.

TAI values range from 0.45 to 1.39 pre-harvest and 0.36 to 1.12 post-harvest with modeled values of 0.79 and 0.64 respectively. The red maple model was the only twig allometric model with a p-value below 0.05. The limited amount of twig data and variability within the twigs weights between individuals in each species led to higher standard errors in the twig models than in leaf models. However, the TAI value bounds aren't nonsensical and fall well within estimates of WAI. Eastern hemlock twigs amount for a much larger portion of the total WAI, but it is possible this is the norm for this species in stands of similar hemlock stocking. Studies looking specifically at fine branch contribution to PAI are sufficiently sparse that there are no specific studies relevant to validate these results. The diameters of these fine branches fall below what TLS can resolve at effective ranges and are well below what can be imaged by DHP pixels.

WAI and clumping-corrected PAI values were found by using the clumping value given in leaf-off conditions, which provided matching WAI values in leaf-off and leaf-on conditions. This gave a WAI of 1.74 pre-harvest and 1.42 post-harvest. These values are estimated by altering the clumping value given by CAN-EYE and assuming the leaf off WAI as $WAI = PAI - (LAIconiferous + LAIdeciduous)$. This gives the plot a maximum range of woody-to-total plant material "α" of 0.17-0.45, falling around a value of $\alpha = 0.22$. Here, $\alpha = WAI/PAI$. These ranges meet those found by Woodgate et al. (2016) and Sea et al. (2011), although the actual modelled value of 0.22 is slightly lower. This is one way of estimating WAI, but it is without direct measurement or other

validation. A viable validation method in the future would be to use bispectral TLS to separate wood and leaf returns (Danson et al., 2014, Li et al., 2013) and/or estimate woody volumes and areas using quantitative structure modeling (QSM, Raumonen et al., 2013, Calders et al., 2015). Another viable, though more time-consuming, method would be to take more detailed wood and branch structure measurements and apply them directly to WAI estimations.

Future Analyses

Best practice for using and understanding vegetation area index values includes seeking good estimates of both LAI and WAI. Simply looking at effective or true PAI values whether from DHP, TLS, or other indirect PAI estimates misses out on key information in a forest. Understanding what portion of the found PAI is actually WAI or LAI helps further understand forest productivity, health, and key climactic trends (Richardson et al., 2010, Reich, 2012).

Use of a plot- or acquisition-specific clumping index or voxelization is key in bringing effective PAI values closer to true PAI values by accounting for between-crown clumping (Woodgate et al., 2017, Zhao et al., 2012, Beland et al., 2014, Jupp et al., 2009, Jonckheere et al., 2004, and Weiss et al., 2004). However, these methods fail to see within-crown clumping caused by fine branches supporting leaves within the leaf crowns. These twigs are a portion of the total WAI that in this study is called TAI. The fine-branch portion of TAI is typically assumed to be a part of the crowns in the between-crown clumping, as the crowns between the gaps are assumed to be leaf clumps (Jupp et al., 2009).

Parsing out fine-branches using a leaf-twig ratio *R* was used in this study and is similar to α used by Sea et al. (2011), Woodgate et al. (2016), and Calders et al. (2018) to determine total WAI within the PAI. More intense destructive sampling such as that performed in this study may be necessary to help better understand fine-branch, within-crown clumping for different species and plot compositions, as these small branches with DHP show up simply as mixed pixels, and typical TLS resolutions may be too small to distinguish them at effective ranges (Armston et al., 2014).

Using α to estimate WAI will help in further separation of PAI and LAI. Simulations are useful in this aspect as they can include known values and can be used to validate methodologies for determining α (Woodgate et al., 2016 and Calders et al., 2018). In the field, using TLS to find woody areas is the most cost-effective methodology to separate wood from leaves, though occlusion at times can make this difficult (Danson et al., 2014, Li et al., 2013, and Armston et al., 2014). QSM and intensive destructive sampling can be used in studies like this in the future to validate the WAI values found and help establish plot *R* and α values (Raumonen et al., 2013, Calders et al., 2015).

CONCLUSION

This study utilized highly detailed destructive sampling, repeat DHP photography, and TLS data to obtain detailed ratios and measurements of leaves, woody material, and fine branches within a mixed temperate forest. The focus of this study on accurate vegetation area indexes and correction of readily available DHP PAI with highly detailed supporting data showed that forest structure is more complex than many studies must assume. Further studies of this nature are needed to develop more accurate, repeatable LAI values that can be used to improve ecological models.

Detailed destructive sampling methodologies were performed on twenty trees in a 50 x 50-m plot and adjacent area in the Harvard Forest. These methodologies followed specially-developed harvesting protocols developed and executed by forestry partners and were performed on *Tsuga canadensis*, *Pinus strobus*, *Quercus rubra*, and *Acer rubrum*. The plot was dominated by eastern hemlock, which provided 55.5 percent of the plot's basal area. Leaf weights, twig weights, specific leaf areas, and specific twig areas were measured and used to find the one-sided leaf area of each of the destructively sampled trees.

Species-specific allometric equations were developed using a log-log relationship of basal area to total one-sided leaf/twig area of each tree. These relationships tended to perform better for leaf areas than twig areas. These allometric relationships are applicable to the four studied species in similar mixed temperate forests. Total plot one-sided leaf area was found by utilizing the allometric equations on each of the 249 live tree stems in the plot to get a total one-sided leaf area of 14,948 m^2 and projected twig/fine branch area

of 1963 m^2. These values were divided by the 50 x 50-m plot area to give LAI and TAI values of 5.98 and 0.78 respectively. These values were bracketed by two-sided standard errors in the allometric equations. This analysis was performed in April 2017 leaf-off conditions, August 2017 pre-harvest conditions, and September 2017 post-harvest, pre-senescence conditions. Allometric equations used were from the destructive sampling in August 2017. A leaf-twig ratio "*R*" was calculated as 12.43 to determine TAI. This value was found by taking the total sampled leaf area to the total sampled projected twig area. TAI found this way was on the lower end of allometric TAI standard error calculations, possibly showing that allometric TAI was overestimated in this case.

DHP PAI values were found to closely match TLS PAI as well as modeled PAI values in leaf-off and leaf-on conditions. All effective PAI values were adjusted using the leaf-off clumping index value obtained from CAN-EYE DHP processing. This value of 0.58 gave a WAI match in leaf-off and leaf-on conditions of 1.71 to 1.74. This gave WAI to PAI ratio values, α, slightly lower than those of Calders et al. (2018) and Woodgate et al. (2016). However, the previous study α values fall within the standard error in this study and Calders et al. (2018) and Woodgate et al. (2016) performed their studies on deciduous forests with different species present. Eastern hemlock was found to be the only tree with a contributing large portion of TAI to WAI. WAI was not independently validated in this study, though this is possible with further processing of the TLS data from pre-harvest conditions.

LAI in leaf off conditions consisted strictly of evergreen eastern hemlock and white pine at 4.42. Just prior to harvest, LAI was found to be 5.98, and post-harvest LAI

dropped to 5.08, simulating a forest disturbance similar to selective logging. WAI decreased by 0.32 due to harvesting, leading to a total PAI loss of around 1.22.

This study is applicable to further estimations of temperate forest PAI, LAI, WAI, and TAI using α and *R* ratios found in this study. Further validation of WAI would also increase confidence in PAItrue calculations after correcting for clumping. Future areas of focus in this realm will involve more detailed destructive sampling in order to lower standard errors in the leaf and twig allometric models, and simulations of DHP and TLS data acquired from mixed temperate forests to develop a further understanding of ratio accuracies.

APPENDIX

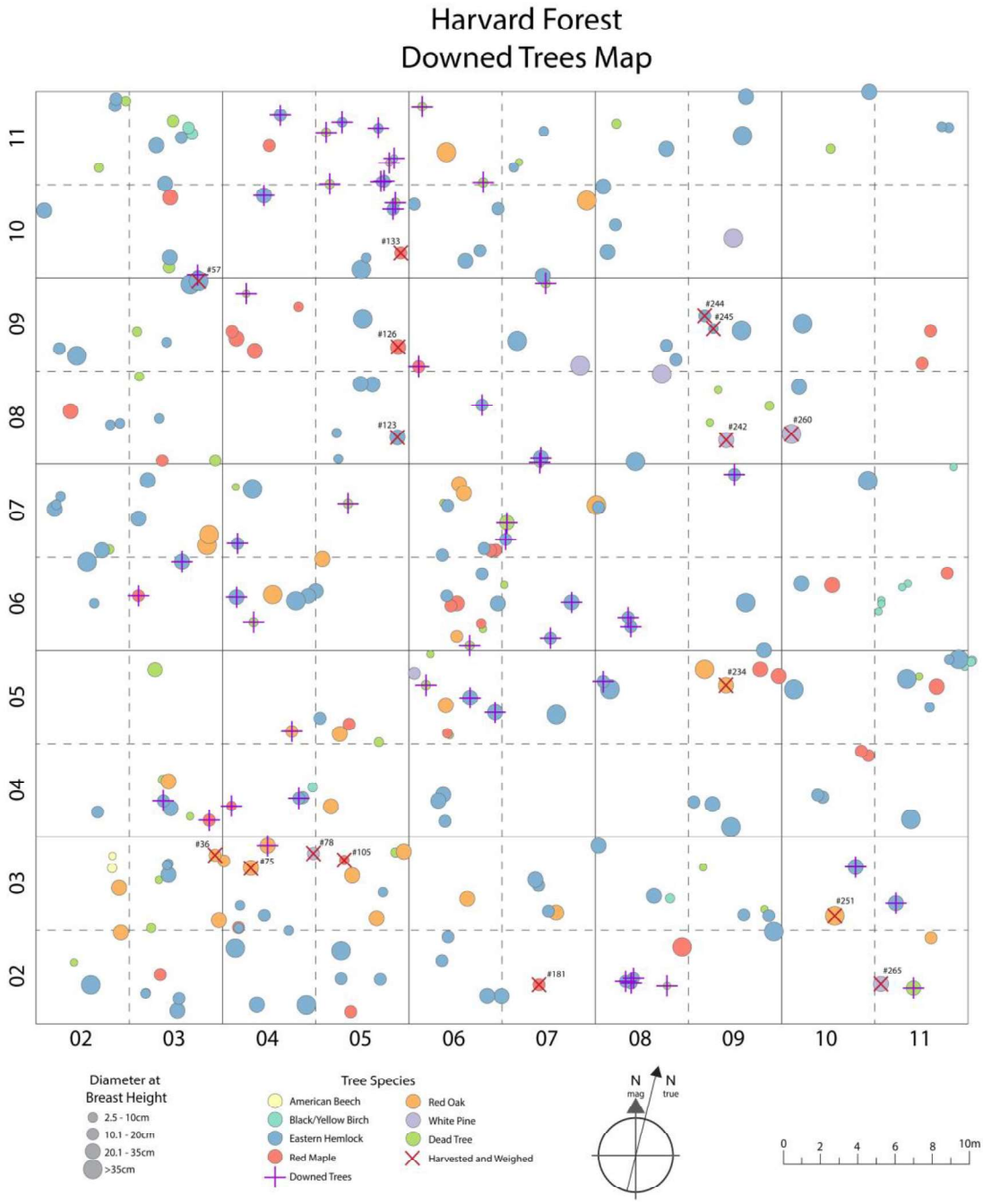

Figure 16. Plot Map. All stems are shown in the plot map laid over the 50x50-m sampling grid.

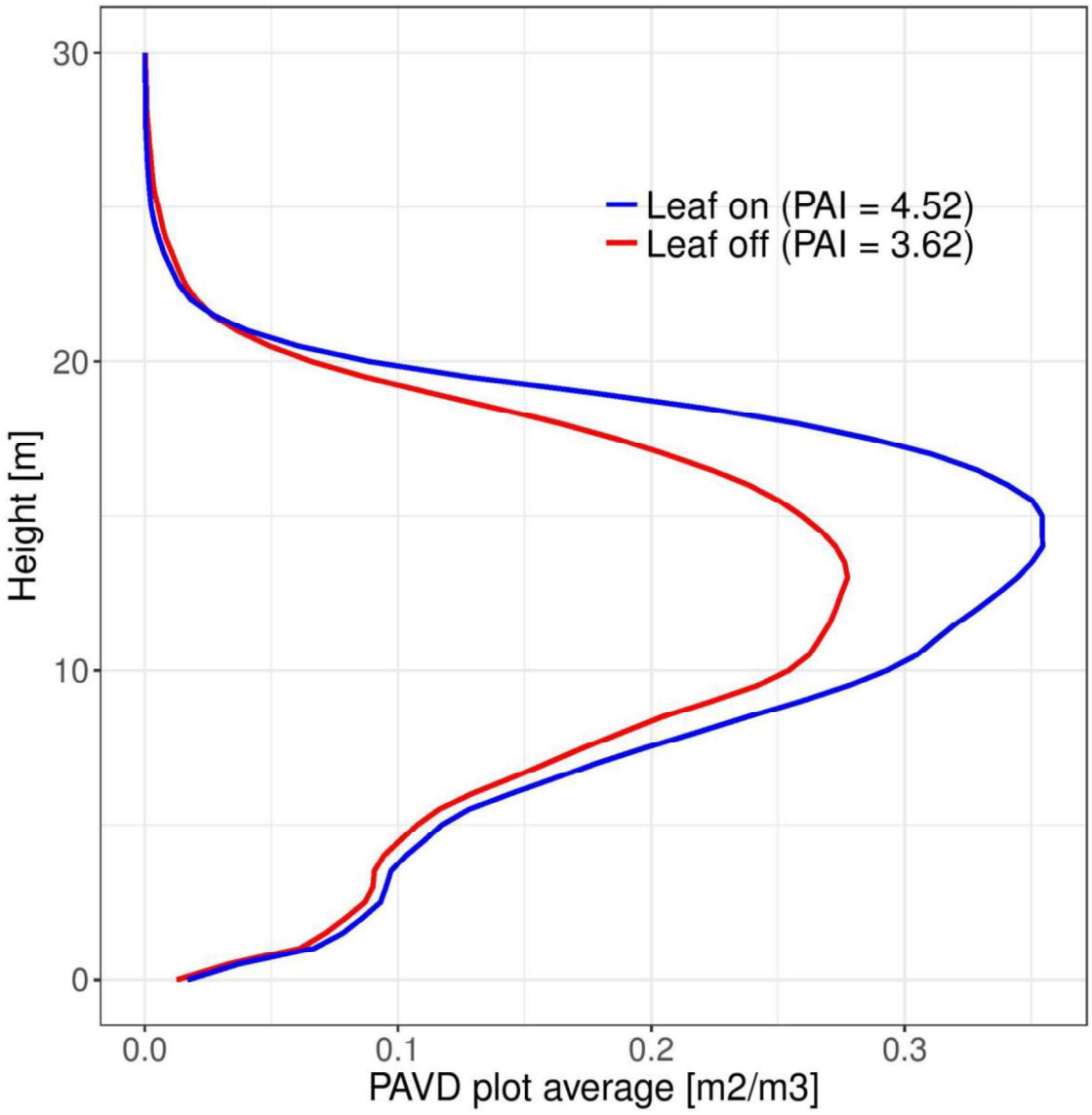

Figure 17. TLS PAVD. A Plant Area Volume Density plot of the 50 x 50-m sampled area produced in pylidar.

Tree Number	Species	DBH (cm)	Column	Row	X Position	Y Position
1	Dead	8.7	2	2	2.01	3.22
2	Red oak	14.9	2	2	4.50	4.83
3	Eastern hemlock	35.6	2	2	2.79	1.95
4	White Birch	2.6	2	3	9.10	3.96
5	White Birch	11.1	2	3	9.04	3.27
6	Red oak	21.9	2	3	9.37	2.22
7	Eastern hemlock	11.2	2	4	13.25	1.31
8	Eastern hemlock	38.6	2	6	22.65	4.59
9	Eastern hemlock	5.5	2	6	23.11	2.52
10	Eastern hemlock	34.9	2	7	25.93	2.43
11	Eastern hemlock	5.5	2	7	26.08	2.80
12	Eastern hemlock	2.6	2	7	26.31	3.25
13	Eastern hemlock	29.2	2	7	28.38	0.36
14	Dead	10.7	2	7	28.88	0.41
15	Eastern hemlock	3	2	8	33.97	2.11
16	Eastern hemlock	3.3	2	8	34.49	2.19
17	Red maple	21	2	8	31.80	2.77
18	Eastern hemlock	10.9	2	9	36.22	1.18
19	Eastern hemlock	50.9	2	9	36.96	0.75
20	Eastern hemlock	29.3	2	10	40.43	3.47
21	Eastern hemlock		2	11	49.30	4.61
22	Dead		2	11	49.83	4.50
23	Eastern hemlock		2	11	49.24	4.24
24	Dead		2	11	48.38	0.91
25	Eastern hemlock	2.6	3	2	0.87	6.58
26	Eastern hemlock	8.1	3	2	0.87	6.58
27	Red maple	18.9	3	2	1.61	7.53
28	Eastern hemlock	16.7	3	2	2.60	6.29
29	Eastern hemlock	34.2	3	2	2.42	5.64
30	Dead	4.4	3	3	6.58	7.67
31	Eastern hemlock	4.5	3	3	7.01	8.46
32	Eastern hemlock	4.7	3	3	7.09	8.53
33	Eastern hemlock	26.2	3	3	7.03	7.85
34	Red oak	28.8	3	3	9.67	5.52
35	Dead	15.4	3	3	6.09	5.11
36	Red oak	19.6	3	3	9.53	8.94
37	Red oak	15	3	3	10.02	8.64
38	Dead	12.3	3	4	11.77	8.02

Tree Number	Species	DBH (cm)	Column	Row	X Position	Y Position
39	Red oak	27.9	3	4	12.02	7.86
40	Eastern hemlock	11.6	3	4	11.79	6.89
41	Eastern hemlock	20.9	3	4	12.14	6.48
42	Dead	7.3	3	4	13.22	6.08
43	Red maple	16.8	3	4	14.21	5.88
44	Dead	59.9	3	5	16.28	8.68
45	Red maple	17.8	3	6	20.48	7.86
46	Eastern hemlock	27.5	3	6	22.76	9.64
47	Eastern hemlock	27.9	3	7	25.46	6.95
48	Eastern hemlock	29.7	3	7	25.95	8.99
49	Red oak	49.8	3	7	29.04	6.14
50	Red oak	43.1	3	7	28.95	5.61
51	Dead	10.6	3	8	30.53	9.67
52	Eastern hemlock	8.2	3	8	31.58	7.43
53	Red maple	15	3	8	31.69	5.19
54	Dead	24.6	3	8	34.50	5.20
55	Dead	12.2	3	9	35.40	7.06
56	Eastern hemlock	37.3	3	9	38.16	9.50
57	Eastern hemlock	40.6	3	9	38.60	9.67
58	Eastern hemlock	5.5	3	9	38.65	10.14
59	Eastern hemlock	8.3	3	9	36.97	6.54
60	Red maple	28.5	3	11	47.13	9.19
61	Eastern hemlock	28.1	3	11	47.05	6.05
62	Dead	22.3	3	11	47.03	5.54
63	Eastern hemlock	31.2	3	12	51.36	6.98
64	Dead	27.2	3	12	52.27	8.30
65	Eastern hemlock	14.3	3	12	52.74	7.49
66	Yellow birch	22.2	3	12	53.10	7.98
67	Yellow birch	25	3	12	53.26	7.64
68	Eastern hemlock	24.4	3	12	51.80	5.04
69	Eastern hemlock	37	4	2	0.66	13.84
70	Red maple	16.6	4	2	0.86	15.03
71	Eastern hemlock	2.9	4	2	0.86	15.13
72	Eastern hemlock	4	4	2	3.54	14.97
73	Eastern hemlock	20.9	4	2	1.76	10.95
74	Eastern hemlock	61.2	4	2	4.20	10.92
75	Red oak	32.8	4	3	6.46	13.18
76	Eastern hemlock	5	4	3	5.92	11.31

Tree Number	Species	DBH (cm)	Column	Row	X Position	Y Position
77	Red oak	24.5	4	3	7.36	14.41
78	White pine	13.9	4	3	9.83	14.05
79	Eastern hemlock	16.6	4	3	7.17	10.77
80	Red maple	4.6	4	4	10.47	11.63
81	Eastern hemlock	18.2	4	4	14.02	12.03
82	Eastern hemlock	17.6	4	4	14.22	12.07
83	Red oak	15.5	4	5	18.64	10.66
84	Eastern hemlock	33.9	4	6	20.71	12.71
85	Dead	12.3	4	6	21.62	11.48
86	Red oak	47.9	4	6	22.53	12.83
87	Eastern hemlock	31.5	4	6	23.80	12.59
88	Eastern hemlock	32	4	6	24.46	12.86
89	Eastern hemlock	28.3	4	6	24.89	13.12
90	Dead	8.8	4	7	25.71	13.73
91	Eastern hemlock	42.3	4	7	26.53	13.48
92	Eastern hemlock	17	4	7	25.74	10.67
93	Red maple	17.3	4	9	35.49	12.04
94	Red maple	21.5	4	9	35.70	11.66
95	Dead	9.2	4	9	36.26	14.11
96	Eastern hemlock	8	4	9	39.05	13.42
97	Red maple	30	4	9	36.60	11.02
98	Eastern hemlock	29.2	4	10	42.16	14.29
99	Red maple	13	4	11	47.45	12.05
100	Eastern hemlock	12.2	4	11	48.07	13.69
101	Eastern hemlock	9.2	5	2	1.34	17.35
102	Eastern hemlock	44.3	5	2	1.29	18.68
103	Eastern hemlock	18.9	5	2	3.39	17.30
104	Red maple	16	5	2	1.80	15.60
105	Red maple	8.1	5	3	6.52	18.70
106	Red oak	24.9	5	3	6.89	17.83
107	Dead	12.1	5	3	9.24	19.11
108	Red oak	23.3	5	3	9.64	19.12
109	Eastern hemlock	10	5	3	8.57	17.02
110	Red oak	26.3	5	3	8.14	15.61
111	Black birch	11	5	4	9.84	17.60
112	Red oak	24.9	5	4	10.76	16.52
113	Eastern hemlock	18.2	5	4	16.85	15.83
114	Eastern hemlock	18.8	5	5	15.22	16.28

Tree Number	Species	DBH (cm)	Column	Row	X Position	Y Position
115	Red oak	20.7	5	5	16.20	15.50
116	Red maple	15.8	5	5	16.73	16.01
117	Dead	18	5	5	18.30	15.09
118	Red oak	25.7	5	6	20.35	19.79
119	Dead	11.1	5	7	26.70	17.83
120	Eastern hemlock	3.7	5	8	31.11	16.66
121	Eastern hemlock	30.2	5	8	32.33	19.19
122	Eastern hemlock	34	5	8	32.95	19.16
123	Eastern hemlock	23.7	5	8	34.27	16.41
124	Eastern hemlock	9	5	8	31.17	15.28
125	Eastern hemlock	53.9	5	9	37.35	17.60
126	Red maple	22.1	5	9	39.32	16.27
127	Dead	18.8	5	10	40.74	19.95
128	Eastern hemlock	8.6	5	10	43.48	20.13
129	Eastern hemlock	12.9	5	10	43.63	20.15
130	Dead	14	5	10	44.22	18.98
131	Eastern hemlock	11.2	5	10	44.11	18.66
132	Eastern hemlock	4.7	5	10	42.69	16.08
133	Red maple	12.9	5	10	44.51	16.33
134	Eastern hemlock	38	5	10	42.26	15.42
135	Dead	12.8	5	11	45.55	17.75
136	Eastern hemlock	7.5	5	11	46.40	18.32
137	Eastern hemlock	6.4	5	11	48.34	18.02
138	Black birch	8.1	5	11	49.17	16.40
139	Dead	2.6	5	11	48.93	16.16
140	Eastern hemlock	17.1	6	2	2.07	24.55
141	Eastern hemlock	17.7	6	2	1.73	23.27
142	Eastern hemlock	29	6	2	4.06	21.41
143	Red oak	31.9	6	3	7.99	21.61
144	Eastern hemlock	20.1	6	4	11.52	21.86
145	Eastern hemlock	24.1	6	4	11.77	22.17
146	White pine	15.7	6	5	15.28	23.69
147	Dead	15.8	6	5	15.89	23.07
148	Dead	8.6	6	5	16.14	24.76
149	Red oak	33	6	5	16.86	21.96
150	Eastern hemlock	21.8	6	5	18.19	22.41
151	Eastern hemlock	26.5	6	5	19.50	21.66
152	Red maple	8.1	6	5	17.02	20.56

Tree Number	Species	DBH (cm)	Column	Row	X Position	Y Position
153	Dead	7.6	6	5	17.15	20.45
154	Eastern hemlock	16.2	6	6	21.99	22.88
155	Red maple	18	6	6	22.19	22.33
156	Red maple	22	6	6	22.50	22.45
157	Eastern hemlock	18.7	6	6	23.86	24.06
158	Red oak	16	6	6	22.49	20.73
159	Dead	14	6	6	23.19	20.26
160	Red maple	7.7	6	6	23.84	21.44
161	Dead	8.4	6	6	23.94	21.15
162	Eastern hemlock	20.1	6	6	24.68	22.48
163	Dead	9.4	6	7	26.83	22.87
164	Eastern hemlock	14.7	6	7	27.04	22.72
165	Red oak	32.2	6	7	27.61	23.79
166	Red oak	26.2	6	7	27.86	23.34
167	Eastern hemlock	19.3	6	7	26.70	20.11
168	Eastern hemlock	12.2	6	7	28.97	20.45
169	Red maple	19.8	6	7	29.29	20.34
170	Red maple	13.6	6	7	29.59	20.37
171	Eastern hemlock	10.8	6	8	33.88	23.15
172	Red maple	17.7	6	9	35.45	20.22
173	Eastern hemlock	14.3	6	10	40.29	23.89
174	Dead	17.2	6	10	43.93	25.05
175	Eastern hemlock	11.8	6	10	44.73	23.69
176	Eastern hemlock	33.9	6	10	42.87	20.88
177	Eastern hemlock	18.5	6	10	43.73	21.44
178	Dead	12.9	6	11	45.70	24.14
179	Red oak	51.8	6	11	46.82	21.57
180	Eastern hemlock	30.8	7	2	-0.03	26.30
181	Red maple	11.3	7	2	1.94	27.02
182	Eastern hemlock	28.7	7	3	6.71	27.59
183	Eastern hemlock	19.1	7	3	6.89	27.33
184	Eastern hemlock	18.1	7	3	7.41	25.99
185	Red oak	30.2	7	3	7.76	25.90
186	Eastern hemlock	34	7	3	10.05	29.40
187	Eastern hemlock	41.1	7	5	17.73	26.47
188	Eastern hemlock	13.8	7	5	20.37	28.30
189	Eastern hemlock	37.2	7	5	20.62	27.85
190	Dead	7.8	7	6	20.12	28.50

Tree Number	Species	DBH (cm)	Column	Row	X Position	Y Position
191	Eastern hemlock	27.9	7	6	23.61	27.51
192	Eastern hemlock	16.4	7	6	22.52	25.64
193	Eastern hemlock	14.5	7	7	25.18	25.88
194	Dead	74.2	7	7	25.21	26.49
195	Red oak	36.9	7	7	29.90	27.71
196	Dead	12.8	7	7	27.00	30.02
197	Eastern hemlock	22.5	7	8	31.97	25.34
198	Eastern hemlock	44.8	7	9	35.71	26.43
199	Eastern hemlock	33.3	7	9	37.12	29.97
200	Dead	11.2	7	9	37.31	29.66
201	White pine	40.3	7	9	38.99	25.29
202	Red oak	50.5	7	10	44.36	28.98
203	Eastern hemlock	3.7	7	11	45.62	25.91
204	Dead	2.8	7	11	45.91	26.19
205	Eastern hemlock	8.3	7	11	47.21	27.84
206	Eastern hemlock	13.7	8	2	1.58	32.19
207	Eastern hemlock	18.6	8	2	1.87	32.09
208	Eastern hemlock	11.6	8	2	2.01	32.36
209	White oak	39.8	8	2	4.51	33.96
210	Dead	7	8	2	3.81	31.99
211	Eastern hemlock	29.5	8	3	8.02	31.77
212	Black birch	12.7	8	3	8.96	31.69
213	Eastern hemlock	19.6	8	6	21.69	31.70
214	Eastern hemlock	19.8	8	6	21.83	31.23
215	Eastern hemlock	17.8	8	7	25.17	32.59
216	Eastern hemlock	51.3	8	8	31.90	30.13
217	White pine	64.7	8	8	33.37	34.59
218	Eastern hemlock	12.2	8	9	38.76	31.37
219	Eastern hemlock	14.2	8	9	39.26	30.61
220	Eastern hemlock	21.5	8	10	40.42	34.78
221	Eastern hemlock	12.6	8	10	41.06	32.81
222	Eastern hemlock	29.5	8	10	40.59	31.27
223	Dead	12.3	8	11	46.11	33.21
224	Eastern hemlock	33.6	8	11	48.66	31.85
225	Dead	7	9	3	5.78	38.31
226	Eastern hemlock	16.4	9	3	7.89	35.80
227	Dead	6	9	3	9.05	36.12
228	Eastern hemlock	16.3	9	3	9.23	35.76

Tree Number	Species	DBH (cm)	Column	Row	X Position	Y Position
229	Eastern hemlock	36.7	9	3	9.40	34.93
230	Eastern hemlock	17	9	4	10.28	36.78
231	Eastern hemlock	34.7	9	4	11.19	36.61
232	Eastern hemlock	47.4	9	4	12.05	35.48
233	Red oak	35.5	9	5	15.82	38.81
234	Red oak	26.8	9	5	16.94	38.03
235	Red maple	27.7	9	5	18.75	38.88
236	Red maple	30	9	5	19.72	38.54
237	Eastern hemlock	41.5	9	6	22.91	37.44
238	Eastern hemlock	30.1	9	6	23.90	35.02
239	Eastern hemlock	16.4	9	7	27.42	39.37
240	Dead	4	9	8	31.14	37.23
241	Dead	2.5	9	8	31.59	39.00
242	White pine	21.5	9	8	31.93	36.25
243	Dead	11.1	9	8	34.29	38.11
244	Eastern hemlock	18.9	9	9	35.85	37.88
245	Eastern hemlock	7.8	9	9	36.32	37.24
246	Eastern hemlock	37.1	9	9	37.70	37.07
247	White pine	64.4	9	10	42.17	36.93
248	Eastern hemlock	30.4	9	11	48.00	39.61
249	Eastern hemlock	42.1	9	11	47.74	37.49
250	Eastern hemlock	21.6	10	3	8.88	43.31
251	Red oak	50.1	10	3	7.61	40.70
252	Eastern hemlock	11.8	10	4	11.89	42.20
253	Eastern hemlock	12.3	10	4	12.16	42.08
254	Red maple	35.5	10	4	14.15	44.47
255	Red maple	35.5	10	4	14.52	44.24
256	Eastern hemlock	40.1	10	5	15.61	42.73
257	Eastern hemlock	32.4	10	6	21.01	43.46
258	Red maple	29.1	10	6	22.62	43.41
259	Eastern hemlock	35.7	10	7	29.49	43.98
260	White pine	41.3	10	8	30.46	41.43
261	Eastern hemlock	33.4	10	8	30.89	44.00
262	Eastern hemlock	55.8	10	9	36.01	42.29
263	Dead	32	10	11	47.50	41.84
264	Eastern hemlock	29	10	11	49.59	44.88
265	White pine	25.4	11	2	0.31	46.98
266	Red oak	17.1	11	2	2.96	49.51

Tree Number	Species	DBH (cm)	Column	Row	X Position	Y Position
267	Dead	40	11	2	1.93	46.75
268	Eastern hemlock	28.8	11	3	6.04	46.34
269	Eastern hemlock	50.6	11	4	11.71	45.84
270	Eastern hemlock	36.4	11	5	16.63	48.32
271	Dead	4.3	11	5	17.37	48.59
272	Eastern hemlock	4.1	11	5	18.98	49.49
273	Red maple	23.1	11	5	18.23	47.99
274	Eastern hemlock	6.6	11	5	17.91	46.94
275	Eastern hemlock	36.5	11	5	19.37	49.40
276	Yellow birch	8.5	11	5	19.79	49.09
277	Yellow birch	13	11	5	20.09	49.35
278	Yellow birch	11.5	11	5	20.17	49.42
279	White Birch	4	11	6	21.46	48.40
280	White Birch	2.58	11	6	20.20	47.09
281	White Birch	5	11	6	20.34	47.48
282	White Birch	3.5	11	6	20.34	47.68
283	White Birch	3.4	11	6	21.76	48.59
284	Red maple	18.8	11	6	23.82	49.10
285	White Birch	3.6	11	7	29.21	49.82
286	Red maple	17.8	11	9	37.92	47.11
287	Red maple	14.2	11	9	37.47	45.41
288	Eastern hemlock	9.9	11	11	48.55	48.08
289	Eastern hemlock	4.9	11	11	48.96	48.06

Table 14. Total Trees in Plot

Tree Number	Species	DBH (cm)	Column	Row	X Position	Y Position	Status
36	Red oak	19.6	3	3	9.53	8.94	Sampled
40	Eastern hemlock	11.6	3	4	11.79	6.89	Downed
43	Red maple	16.8	3	4	14.21	5.88	Downed
45	Red maple	17.8	3	6	20.48	7.86	Downed
46	Eastern hemlock	27.5	3	6	22.76	9.64	Downed
57	Eastern hemlock	40.6	3	9	38.60	9.67	Sampled
58	Eastern hemlock	5.5	3	9	38.65	10.14	Downed
75	Red oak	32.8	4	3	6.46	13.18	Sampled
78	White pine	13.9	4	3	9.83	14.05	Sampled
80	Red maple	4.6	4	4	10.47	11.63	Downed
81	Eastern hemlock	18.2	4	4	14.02	12.03	Downed
83	Red oak	15.5	4	5	18.64	10.66	Downed
84	Eastern hemlock	33.9	4	6	20.71	12.71	Downed
85	Dead	12.3	4	6	21.62	11.48	Downed
92	Eastern hemlock	17	4	7	25.74	10.67	Downed
95	Dead	9.2	4	9	36.26	14.11	Downed
98	Eastern hemlock	29.2	4	10	42.16	14.29	Downed
100	Eastern hemlock	12.2	4	11	48.07	13.69	Downed
105	Red maple	8.1	5	3	6.52	18.70	Sampled
119	Dead	11.1	5	7	26.70	17.83	Downed
123	Eastern hemlock	23.7	5	8	34.27	16.41	Sampled
126	Red maple	22.1	5	9	39.32	16.27	Sampled
127	Dead	18.8	5	10	40.74	19.95	Downed
128	Eastern hemlock	8.6	5	10	43.48	20.13	Downed
129	Eastern hemlock	12.9	5	10	43.63	20.15	Downed
130	Dead	14	5	10	44.22	18.98	Downed
131	Eastern hemlock	11.2	5	10	44.11	18.66	Downed
133	Red maple	12.9	5	10	44.51	16.33	Sampled
135	Dead	12.8	5	11	45.55	17.75	Downed
136	Eastern hemlock	7.5	5	11	46.40	18.32	Downed
137	Eastern hemlock	6.4	5	11	48.34	18.02	Downed
138	Black Birch	8.1	5	11	49.17	16.40	Downed
139	Dead	2.6	5	11	48.93	16.16	Downed
147	Dead	15.8	6	5	15.89	23.07	Downed
150	Eastern hemlock	21.8	6	5	18.19	22.41	Downed
151	Eastern hemlock	26.5	6	5	19.50	21.66	Downed
159	Dead	14	6	6	23.19	20.26	Downed
171	Eastern hemlock	10.8	6	8	33.88	23.15	Downed

Tree Number	Species	DBH (cm)	Column	Row	X Position	Y Position	Status
172	Red maple	17.7	6	9	35.45	20.22	Downed
174	Dead	17.2	6	10	43.93	25.05	Downed
178	Dead	12.9	6	11	45.70	24.14	Downed
181	Red maple	11.3	7	2	1.94	27.02	Sampled
188	Eastern hemlock	13.8	7	5	20.37	28.30	Downed
191	Eastern hemlock	27.9	7	6	23.61	27.51	Downed
192	Eastern hemlock	16.4	7	6	22.52	25.64	Downed
193	Eastern hemlock	14.5	7	7	25.18	25.88	Downed
194	Dead	74.2	7	7	25.21	26.49	Downed
196	Dead	12.8	7	7	27.00	30.02	Downed
197	Eastern hemlock	22.5	7	8	31.97	25.34	Downed
200	Dead	11.2	7	9	37.31	29.66	Downed
206	Eastern hemlock	13.7	8	2	1.58	32.19	Downed
207	Eastern hemlock	18.6	8	2	1.87	32.09	Downed
208	Eastern hemlock	11.6	8	2	2.01	32.36	Downed
210	Dead	7	8	2	3.81	31.99	Downed
213	Eastern hemlock	19.6	8	6	21.69	31.70	Downed
214	Eastern hemlock	19.8	8	6	21.83	31.23	Downed
234	Red oak	26.8	9	5	16.94	38.03	Sampled
239	Eastern hemlock	16.4	9	7	27.42	39.37	Downed
242	White pine	21.5	9	8	31.93	36.25	Sampled
244	Eastern hemlock	18.9	9	9	35.85	37.88	Sampled
245	Eastern hemlock	7.8	9	9	36.32	37.24	Sampled
250	Eastern hemlock	21.6	10	3	8.88	43.31	Downed
251	Red oak	50.1	10	3	7.61	40.70	Sampled
260	White pine	41.3	10	8	30.46	41.43	Sampled
265	White pine	25.4	11	2	0.31	46.98	Sampled
267	Dead	40	11	2	1.93	46.75	Downed
268	Eastern hemlock	28.8	11	3	6.04	46.34	Downed

Table 15. Trees Harvested

Tree	Branch	Section	Weight (g)	Area (cm2)
Red maple 126	2		8.5	78.92
Red maple 126	3		2.42	23.39
Red maple 126	5		1.9	17.85
Red maple 126	6		8.23	71.64
Red maple 126	7		1.99	20.48
Red maple 126	8		6.08	45.76
Red maple 126	9		2.23	20.33
Red maple 126	top		18.66	114.15
Red maple 133	1		9.49	96.74
Red maple 133	2		0.25	2.86
Red maple 133	3		0.76	6.13
Red maple 133	top		1.97	17.39
Red oak 75	1		20.57	129.58
Red oak 75	2		17.06	109.32
Red oak 75	5		7.44	51.46
Red oak 75	8		0.63	4.09
Red oak 75	top		1.18	5.99
Red oak 234	2		16.4	103.01
Red oak 234	4		11.74	68.25
Red oak 234	5		14.85	79.51
Red oak 234	7		10.74	60.06
Red oak 234	8		6.53	40.99
Red oak 234	9		6.61	43.45
Red oak 234	10		2.42	13.47
Red oak 234	top		21.62	99.94
White pine 242	1	7	1.19	14.42
White pine 242	1	13	3.16	22.15
White pine 242	1	14	0.92	11.79
White pine 242	1	15	0.32	4.54
White pine 242	1	16	0.77	9.40
White pine 242	1	17	1.08	12.11
White pine 242	2	13	3.23	23.11
White pine 265	1	12	1.08	14.86
White pine 265	1	13	12.37	92.99
White pine 265	1	17	5.99	48.68
Eastern hemlock 57	1	11	5.053	79.21
Eastern hemlock 57	1	12	4.047	100.25
Eastern hemlock 57	1	13	3.566	61.63
Eastern hemlock 57	1	15	7.441	107.01

Tree	Branch	Section	Weight (g)	Area (cm2)
Eastern hemlock 57	1	16	4.156	59.84
Eastern hemlock 57	1	18	4.275	58.79
Eastern hemlock 57	1	20	3.397	48.17
Eastern hemlock 123	1	6	5.017	60.23
Eastern hemlock 123	1	8	2.558	55.18
Eastern hemlock 123	1	9	3.59	88.23
Eastern hemlock 123	1	10	4.046	67.05
Eastern hemlock 123	1	11	4.736	57.37
Eastern hemlock 123	1	12	4.685	80.01
Eastern hemlock 123	1	13	3.973	76.41
Eastern hemlock 123	1	14	7.736	98.78
Eastern hemlock 123	1	3	2.455	48.55
Eastern hemlock 123	1	6	2.468	51.99
Eastern hemlock 123	1	9	1.491	28.58
Eastern hemlock 123	1	14	0.669	15.64

Table 16. Twig Samples

BIBLIOGRAPHY

Armston J, Newnham G, Strahler A, Scaaf C, Danson M (2014) A comparison of terrestrial laser scanning instruments for assessing forested ecosystems. *ForestSAT 2014*.

Asner GP, Braswell BH, Schimel DS, Wessman CA (1998) Ecological research needs from multiangle remote sensing data. *Remote Sensing of Environment*, **63**, 155-165.

Asner GP, Scurlock JMO, Hicke JA (2003) Global synthesis of leaf area index observations: implications for ecological and remote sensing studies. *Global Ecology & Biogeography*, **12**, 191-205.

Beland M, Baldocchi D, Widlowski J, Fournier R, Verstraete M (2014) On seeing the wood from the leaves and the role of voxel size in determining leaf area distribution of forests with terrestrial LiDAR. *Agricultural and Forest Meteorology*, **184**, 82-97.

Bequet R, Campioli M, Kint V, Vansteenkiste D, Muys B, Ceulemans R (2011) Leaf area index development in temperate oak and beech forests is driven by stand characteristics and weather conditions. *Trees*, **25**, 935-946.

Bondeau A, Kicklighter DW, Kaduk J (2008) Comparing global models of terrestrial net primary productivity (NPP): importance of vegetation structure on seasonal NPP estimates. *Global Change Biology*, **5(S1)**, 25-34.

Boring LR, Monk CD, Swank WT (1981) Early regeneration of a clear-cut southern Appalachian forest. *Ecology*, **65**, 1244-1253.

Calders K, Newnham G, Burt A, Murphy S, Raumonen P, Herold M, Culvenor D, Avitabile V, Disney M, Armston J, Kaasalainen M (2015) Nondestructive estimates of above-ground biomass using terrestrial laser scanning. *Methods in Ecology and Evolution*, **6**, 198-208.

Calders K, Origo N, Disney M, Nightingale J, Woodgate W, Armston J, Lewis P (2018) Variability and vias in active and passive ground-based measurements of effective plant, wood and leaf area index. *Agricultural and Forest Meteorology*, **252**, 231-240.

Chen J, Rich P, Gower S, Norman J, Plummer S (1997) Leaf area index of boreal forests: Theory, techniques, and measurements. *Journal of Geophysical Research*, **102**, 4262-443.

Chen JM and Black TA (1992) Defining leaf area index for non-flat leaves. *Plant, Cell & Environment*, **151**, 421-429.

Douglas ES, Martel J, Li Z, Howe G, Hewawasam K, Marshall RA, Schaaf CL, Cook TA, Newnham GJ, Strahler A, Chakrabarti S (2015) Finding leaves in the forest: The dual-wavelength Echidna lidar. *IEEE Geoscience and Remote Sensing Letters*, **12** 776-780.

Fang H, Li W, Wei S, Jiang C (2014) Seasonal variation of leaf area index (LAI) over paddy rice fields in NE China: Intercomparison of destructive sampling, LAI-2200, digital hemispherical photography (DHP), and AccuPAR methods. *Agricultural and Forest Meteorology*, **198**, 126-141.

Fang H, Wenjuan L, Shanshan W, Chongya J (2014) Seasonal variation of leaf area index (LAI) over paddy rice fields in NE China: Intercomparison of destructive sampling, LAI-2200, digital hemispherical photography (DHP), and AccuPAR methods. *Agricultural and Forest Meteorology*, **198**, 126-141.

Forkel M, Carvalhais N, Rodenbeck C, Keeling R, Heimann M, Thonicke K, Zaehle S, Reichstein M (2016) Enhanced seasonal CO2 exchange caused by amplified plant productivity in northern ecosystems. *Science*, **351**, 696-699.

Garrigues S, Shabanov NV, Swanson K, Morisette JT, Baret F, Myneni RB (2008) Intercomparison and sensitivity analysis of Leaf Area Index retrievals form LAI-2000, AccuPAR, and digital hemispherical photography over croplands. *Agricultural and Forest Meteorology*, **148**, 1193-1209.

GCOS (2011) Systematic observation requirements for satellite-based data products for climate. *WM Organisation*, **154**.

Gower S, Kucharik C, Norman J (1999) Direct and indirect estimation of leaf area index fAPAR and net primary production of terrestrial ecosystems. *Remote Sensing of the Environment*, **70**, 29-51.

Graven HD, Keeling RF, Piper SC, PAtra PK, Stephens BB, Wofsy SC, Welp LR, Sweeney C, Tans PP, Kelley JJ, Daube BC, Kort EA, Santoni GW, Bent JD (2013) Enhanced seasonal exchange of CO2 by northern ecosystems since 1960. *Science*, **341**, 1085-1089.

Hancock S, Essery R, Reid T, Carle J, Baxter R, Rutter N, Huntley B (2014) Characterizing forest gap fraction with terrestrial lidar and photography: An examination of relative limitations. *Agricultural and Forest Meteorology*, **189-190**, 105-114.

Howe GA, Hewawasam K, Doglas ES, Martel J, Li Z, Strahler A, Scaaf C, Cook TA, Chakrabarti S (2015) Capabilities and performance of dual-wavelength Echidna® Lidar. *Journal of Applied Remote Sensing*, **9**.

Hyde P, Dubaya R, Walker W, Blair JB, Hofton M, Hunsaker C (2006) Mapping forest structure for wildlife habitat analysis using multi-sensor (LiDAR, SAR/InSAR, ETM+, Quickbird) synergy. *Remote Sensing of Environment*, **106**, 63-73.

Jonckheere I, Flec S, Nackaerts K, Muys B, Coppin P, Weiss M, Baret F (2004) Review of methods for in situ leaf area index determination Part I. Theories, sensors and hemispherical photography. *Agricultural and Forest Meteorology*, **121**, 19-35.

Jupp DLB, Culvenor DS, Lovell JL, Newnham GJ, Strahler AH, Woodcock CE (2009) Estimating forest LAI profiles and structural parameters using a ground-based laser called 'Echidna'. *Tree Physiology*, **29**, 171-181.

Khomik M, Williams CA, Vanderhoof MK, MacLean RG, Dillen SY (2014) On the causes of rising gross ecosystem productivity in a regenerating clearcut environment: leaf area vs species composition. *Tree Physiology*, **34**, 686-700.

Law BE, Cescatti A, Baldocchi DD (2001) Leaf area distribution and radiative transfer in open-canopy forests: implications for mass and energy exchange. *Tree Physiology*, **21**, 777-787.

Li Z, Douglas E, Strahler A, Schaaf C, Yang X, Wang Z, Yao T, Zhalo F, Saenz EJ, Paynter I, Woodcock CE, Chakrabarti S, Cook T, Martel J, Howe G, Jupp DLB, Culvenor DS, Newnham GJ, Lovell JL (2013) Separating leaves from trunks and branches with dual-wavelength terrestrial lidar scanning. *International Geoscience and Remote Sensing Symposium*, 3383-3386.

Li Z, Jupp DLB, Strahler AH, Schaaf CB, Howe G, Hewawasam K, Douglas ES, Chakrabarti S, Cook TA, Paynter I, Saenz EJ, Schaefer M (2016) Radiometric calibration of a dual-wavelength full-waveform terrestrial lidar. *Sensors*, **16**, 1-24.

Li Z, Strahler AH, Hutyra L, Jupp D, Schaaf C, Woodcock C (2015) Advances in measuring forest structure by terrestrial laser scanning with the dual wavelength Echidna Lidar (DWEL). *ProQuest Dissertations and Theses*.

Marks PL (1974) The role of pin cherry (*Prunus pensylvanica*) in the maintenance of stability in northern hardwood ecosystems. *Ecological Monographs*, **44**, 73-88.

Martin PH, Newton AC, Pfeifer M, Khoo MS, Bullock JM (2015) Impacts of tropical selective logging on carbon storage and tree species richness: A meta-analysis. *Forest Ecology and Management*, **356**, 224-233.

Medjibe VP, Putz FE, Starkey MP, Ndouna AA, Memiaghe HR (2011) Impacts of selective logging on above-ground forest biomass in the Monts de Cristal in Gabon. *Forest Ecology and Management*, **262**, 1799-1806.

Myneni RB, Nemani RR, Running SW (1997) Estimation of global leaf area index and absorbed PAR using radiative transfer models. *IEEE Transaction on Geoscience and Remote Sensing*, **23**, 1380-1393.

Nemani RR, Keeling CD, Hashimoto H, Jolly WM, Piper SC, Tucker CJ, Myneni RB, Running SW (2003) Climate-driven increases in global terrestrial net primary production from 1982 to 1999. *Science*, **300**, 1560-1563.

Neumann HH, Den Hartog G (1989) Leaf area measurements based on hemispheric photographs and leaf-litter collection in a deciduous forest during autumn leaf-fall. *Agricultural and Forest Meteorology*, **45**, 325-345.

Niinemets U (1997) Distribution patterns of foliar carbon and nitrogen as affected by tree dimensions and relative light conditions in the canopy of *Picea abies*. *Trees*, **11**, 144-154.

Raumonen P, Kaasalainen M, Akerblom M, Kaasalainen S, Kaartinen H, Vastaranta M, Holopainen M, Disney M, Lewis P (2013) Fast automatic precision tree models from terrestrial laser scanner data. *Remote Sensing*, **5**, 491-520.

Reich PB (2012) Key canopy traits drive forest productivity. *Proceedings of the Royal Society B: Biological Sciences*, **279**, 2128-2134.

Running SW (1984) Microclimate control of forest productivity: Analysis by computer simulation of annual photosynthesis/transpiration balance in different environments. *Agricultural and Forest Meteorology*, **32**, 267-288.

Sea WB, Choler P, Beringer J, Weinmann RA, Hutley LB, Leuning R (2011) Documenting improvement in leaf area index estimates from MODIS using hemispherical photos for Australian savannas. *Agricultural and Forest Meteorology*, **151**, 1453-1461.

Song C, Dickinson MB (2008) Extracting forest canopy structure from spatial information of high resolution optical imagery: tree crown size versus leaf area index. *International Journal of Remote Sensing*, **29**, 5605-5622.

Strahler A, Schaaf C, Orwig D, Barker-Plotkin A, Frank F, Weiskittel A, MacFarlane D, Radtke P (2017) Virtual tree volume and aboveground biomass retrieval from TLS calibrated by destructive sampling at Harvard Forest. *SilviLaser 2017*.

Templer PH (2013) Limits on carbon uptake by plants. *Nature Climate Change*, **3**, 184-185.

Templer PH, Reinmann AB (2011) Multi-factor global change experiments: what have we learned about terrestrial carbon storage and exchange? *New Phytologist,* **192**, 797.

Watson (1947) Growth of Field Crops: I. Variation in net assimilation rate and leaf area between species and varieties and with and between years. *Annals of Botany*, **11**, 41-76.

Weiss M, Baret F, Smith GJ, Jonckheere I, Coppin P (2004) Review of methods for in situ leaf area index (LAI) determination Part II. Estimation of LAI, errors and sampling. *Agricultural and Forest Meteorology*, **121**, 37-53.

Welles JM, Norman JM (1991) Instrument for indirect measurement of canopy architecture. *Agronomy Journal*, **83**, 818-825.

White RH, Ross RH (2014) Wood and Timber Condition Assessment Manual. **2**.

Woodgate W, Armston JD, Disney M, Jones SD, Suarez L, Hill MJ, Wilkes P, Soto-Berelov M (2016) Quantifying the impact of woody material on leaf area index estimations from hemispherical photography using 3D canopy simulations. *Agricultural and Forest Meteorology*, **226-227**, 1-12.

Woodgate W, Armston JD, Disney M, Suarez L, Jones SD, Hill MJ, Wilkes P, Soto-Berelov M (2017) Validating canopy clumping retrieval methods using hemispherical photography in a simulated Eucalypt forest. *Agricultural and Forest Meteorology*, **247**, 181-193.

Woodgate W, Jones SD, Suarez L, Hill MJ, Armston JD, Wilkes P, Soto-Berelov M, Haywood A, Mellor A (2015) Understanding the variability in ground-based methods for retrieving canopy openness, gap fraction, and leaf area index in diverse forest systems. *Agricultural and Forest Meteorology*, **205**, 83-95.

Zhao F, Strahler AH, Schaaf CL, Yao T, Yang X, Wang Z, Schull MA, Roman MO, Woodcock CE, Olofsson P, Ni-Meister W, Jupp DLB, Lovell JL, Culvenor DS, Newnham GJ (2012) Measuring gap fraction, element clumping index and LAI in Sierra Forest stands using a full-waveform ground-based lidar. *Remote Sensing of Environment*, **125**, 73-79.

Zhao F, Yang X, Schull MA, Roman-Colon MO, Yao T, Wang Z, Zhang Q, Jupp DLB, Lovell JL, Culvenor DS, Newnham GJ, Richardson AD, Ni-Meister WN, Schaaf CL, Woodcock CE, Strahler AH (2011) Measuring effective leaf area index, foliage profile, and stand height in New England forest stands using a full waveform ground-based lidar. *Remote Sensing of Environment*, **115**, 2954-2964.

CURRICULUM VITAE